Next Generation Anodes for Lithium-Ion Batteries
Second Quarter Progress Report 2019

Jack Vaughey, Point-of-Contact
Argonne National Laboratory
9700 South Cass Avenue
Argonne, IL 60439
Phone: (630) 252-8885
E-mail: vaughey@anl.gov

Brian Cunningham, DOE-EERE-VTO Technology Manager
U.S. Department of Energy, Battery R&D
Phone: (202) 287-5686
E-mail: brian.cunningham@ee.doe.gov

Table of Contents

Silicon Deep Dive Overview

Project Introduction

Silicon has received significant attention as an alternative to the graphitic carbon negative electrodes presently used in a lithium-ion battery due to its high capacity and availability. Compared to graphitic carbons, elemental silicon's capacity is nearly an order of magnitude higher (~3600 mAh/g silicon vs 372 mAh/g Graphite). However, several problems have been identified that limit its utility including a large crystallographic expansion (~320%) upon full lithiation, slow lithium diffusion, and high reactivity at high states of charge. Together these physical properties result in particle cracking, particle isolation, electrolyte reactivity, and electrode delamination issues. These chemical reactivity and volume changes are manifested in SEI stability (calendar and life studies) and cycling efficiency issues for the cell. Because of the technological advances possible if a silicon anode can be designed and proven, researchers in multiple disciplines have pushed to understand these physical issues and advance the field and create a viable silicon-based electrode.

Next Generation Anodes for Lithium-Ion Batteries, also referred to as the silicon Deep Dive Program, is a consortium of five National Laboratories assembled to tackle the barriers associated with development of an advanced lithium-ion negative electrode based upon silicon as the active material. This research program has several goals including (1) evaluating promising silicon materials that can be either developed by a team member or obtained in quantities sufficient for electrode preparation by the consortiums facilities, (2) developing a composite silicon-Gr electrode that meets BatPac specifications, and (3) executing full cell development strategies that leverage DOE-EERE-VTO investments in electrode materials and characterization. The primary objective of this program is to understand and eliminate the barriers to implementation of a silicon based anode in a lithium-ion cell. The Five National Laboratories (ANL, NREL, LBNL, ORNL, and SNL) involved are focused on a single program with continuous interaction, clear protocols for analysis, and targets for developing both an understanding and a cell chemistry associated with advance negative electrodes for lithium-ion cells. This undertaking is a full electrode/full cell chemistry project with efforts directed at understanding and developing the chemistry needed for advancing silicon-based anodes operating in full cells. Materials development efforts include active material development, binder synthesis, coatings, safety, and electrolyte additives. Efforts include diagnostic research from all partners, which span a wide range of electrochemical, chemical and structural characterization of the system across length- and time-scales. Specialized characterization techniques developed with DOE-EERE-VTO funding, include neutrons, MAS-NMR, optical, and X-ray techniques being employed to understand operation and failure mechanisms in silicon-based anodes. In addition, several strategies to mitigate lithium loss are being assessed. The project is managed as a single team effort spanning the Labs, with consensus decisions driving research directions and toward development of a functioning stable silicon-based electrode.

The silicon Deep Dive project seeks to identify the limiting factors of silicon-based electrodes that need to be overcome to produce a viable functioning LIB electrode and full cell. The issues include understanding and controlling silicon surface chemistry, lithium loss due to side reactions, active material interactions, and the role of electrolyte stability. The goal of the project is utilize our understanding of silicon and silicide reactivity, electrode formulation, and binder and electrolyte formulations, to design a functioning silicon-based electrode for a lithium-ion cell that meets DOE-EERE goals. Combined with the SEISta's efforts focused on interfacial reactivity, composition, and stability, key variables can be isolated and studied to improve the performance of a silicon-based cell. This key interaction is maintained and accomplished through joint meetings, face to face discussions, and extensive collaborations between the teams.

Current Deep Dive Goals:

Q1   Demonstrate improved cycling efficiency of a silicon-based electrode that incorporates either an inorganic or organic surface modification compared to uncoated silicon baseline

Q2   Exhibit a binder designed to strongly interact with the silicon particle surface that shows enhanced cycling stability versus an LiPAA baseline.

Q3   Demonstrate that controlling lithium inventory in a full cell can extend cycle life of a silicon-based electrode by at least 10%.

Q4   Construct and evaluate cells based on optimizing lithium inventory, binder, electrolyte formulation, and testing protocol to achieve a 300 Wh/kg cell design.

Approach

Oak Ridge National Laboratory (ORNL), National Renewable Energy Laboratory (NREL), Pacific Northwest National Laboratory (PNNL), Lawrence Berkeley National Laboratory (LBNL), and Argonne National Laboratory (ANL) have teamed together to form an integrated program. Technical targets have been developed and regular communications have been established. Throughout the program, there is a planned focus on understanding, insights into, and advancement of, silicon-based materials, electrodes, and cells. All anode advancements will be verified based on life and performance of full cells. Toward that end, baseline siliconbased materials, electrodes, and cells have been adopted, along with full cell testing protocols.
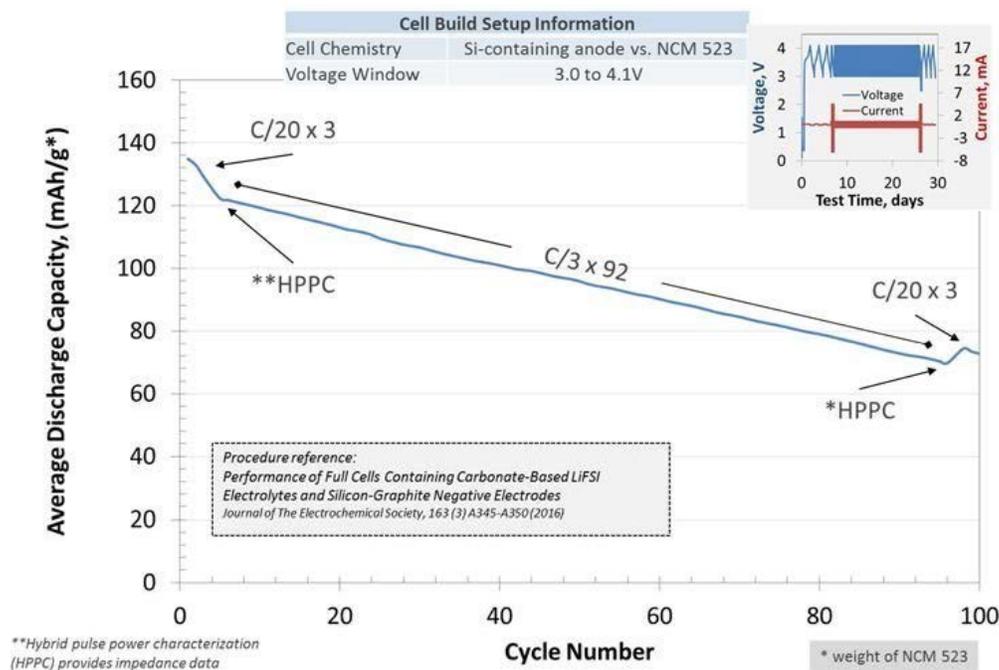

Figure 1. Full cell testing protocol.

In examining improvements, changes to the baseline cell technology will be minimized. As an example, silicon active material coating improvements will be verified on baseline silicon materials in electrodes fabricated by the battery research facilities. All other components in the prototype cells (i.e. positive electrode, separator, and electrolyte) will be from the baseline technology. While there are many testing protocols that can be utilized to benchmark the baseline technology, this program has adopted a testing protocol from the literature that has worked well for lithium-ion cells with silicon containing anodes. Shown pictorially in **Figure** 1 the test starts with three slow (C/20) formation cycles, an HPPC cycle, and then the C/3 aging cycles. The test ends with another HPPC cycle and three more slow (C/20) cycles. All constant current cycling is symmetric between charge and discharge rates. The tests are run at 30°C. If there is little or no aging in the first 100 cycles, the protocol can be repeated. This protocol effectively examines capacity, impedance, and aging effects in about a month's worth of testing. As the program matures, materials developments will be incorporated into baseline silicon-based materials, electrodes, and cells. Scale-up of materials, incorporation of materials advancements into electrodes and prototype cells, and characterization and testing of cells, as well as evaluation of safety and abuse tolerance are part of a wide range of integrated studies supported by battery research facilities at the National Labs working closely with the program. These research facilities include the Battery Abuse Testing Laboratory (BATLab), the Battery Manufacturing Facility (BMF), the Cell Analysis, Modeling, and Prototyping (CAMP) facility, the Materials Engineering Research Facility (MERF), and the Post-Test Facility (PTF). At the present time the baseline silicon is from Paraclete Energy (Chelsea, MI).

The fundamental understanding of silicon-based electrode active materials is based on extensive electrochemical and analytical diagnostic studies on components, electrodes, and cells conducted within the program. This effort contains in-situ and ex-situ studies on full and specialty cells, including reference electrode cells. Overall, the diagnostic studies are intended to help establish structure-composition-property relationships, including lithium-reactivity at the silicon surface and bulk transport and kinetic phenomena. Further, they should form the basis for accurately assessing component and electrode failure modes and lay a path for advancements.

Supported by diagnostic studies, materials development on silicon-based materials, electrodes, and cells is being conducted to enhance interfacial stability, accommodate intermetallic volume changes, and improve overall performance and life. Key to this effort is the development and testing of coatings and additives designed to modify and stabilize the dynamic silicon-electrolyte interface. Further, functional polymer binders designed to accommodate volume changes, increase conductivity, and improve adherence are being developed and analyzed. Finally, the program is exploring active material development, including high-energy silicon and silicide materials, development of additional lithium inventory additives, and use of designer passivation materials.

Communication of programmatic progress to battery community is critical. This will generally be accomplished through publications, presentations, reports, and reviews. Further, the program is open to industrial participation and/or collaboration that does not limit program innovation or the free flow of information. Finally, this program is highly integrated with our sister program on SEI-Stabilization (SEISta). In general, SEISta is focused on the development and characterization of model systems, thin-film well-defined active area electrodes on which it is easier to extract fundamental information on lithium-silicon phase formation, lithium transport, and interfacial phenomena (e.g. SEI formation and growth).

Milestone FY2019Q2

Exhibit a binder designed to strongly interact with the silicon particle surface that shows enhanced cycling stability versus a LiPAA program baseline.

Within the DeepDive Silicon effort, we have a multi-team effort seeking to understand how the binder chemistry -silicon surface properties interact to create stable electrodes, reproducible laminates, and stable electrochemical properties. Lu Zhang (ANL) has been studying the role of pH on the binding ability of PAA-based binder systems, an effort led by Beth Armstrong and Gabe Veith (ORNL) has been looking at how the pH of the solution used to cast the binder and silicon slurry changes with the surface properties of the underlying silicon surface, and John Zhang's group (ANL) has been investigating the coupling chemistry of organic species attachment to the various surface groups available on a silicon surface. Combined these teams represent a three-pronged study of how an electrode based on silicon is created and can be optimized for electrochemical testing and properties.

Summary: In Q2, we have a focus on understanding the interface between the active materials and the system level components such as the current collector, binder, and conductive additives. In this quarter John Zhang's group has continued their studies on identifying the optimal surfaces for attaching via Si-O bonds organic species. Electrochemical work by Wenquan Lu (ANL), Manuel Schnabel (NREL/SEISta), among others has shown that the silica layer on silicon can be porous to lithium (on cycling) however intentional densification of the layer has deleterious effects on properties, until breakthrough or a corrosion reaction creates a better pathway. John Zhang and Nate Neale's (NREL/SEIsta) group have been working on changing the surface termination on silicon from two different perspectives to arrive at hydride termination. Neales group has earlier shown that the materials could be produced on by a gas phase reaction and demonstrated that these materials could be used to design a new surface termination. In collaboration with Zhangs group, the effort
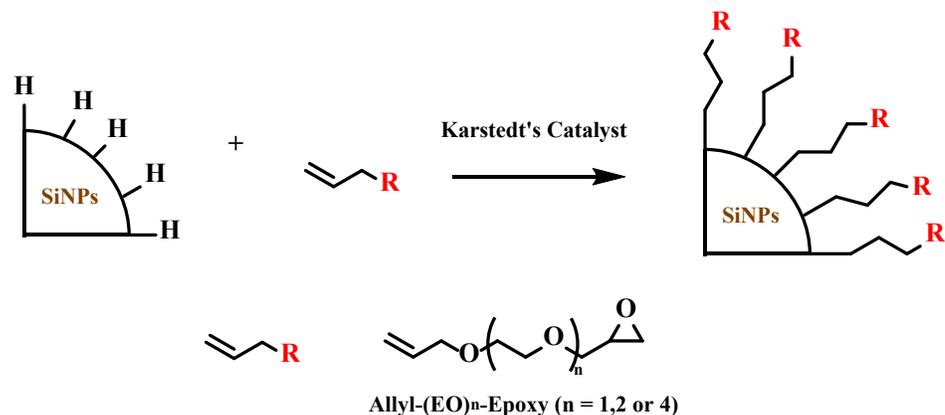

Figure 2. Demonstration of functionalizing the surface of silicon by building in better chemical reactivity to the surfaces and organic molecules.

has expanded to using commercial silicon naturally passivated by silica as a starting material and using silica dissolution methods to terminate the surface as needed with protons. In this quarter Zhangs group tested four different sources and identified an Alfa-Aesar silicon as the most promising as it had the least amount of organic contamination. Using this and the silicon hydride nanoparticles developed by Neale Group, a series of catalytic reactions have been tested and evaluated to covalently attach organic groups to the protonated surface. To date Zhang et al., has demonstrated that various PEO-like attachments can be readily affixed to

the surface via a displacement reaction involving the proton. These are similar reactions to the attachment of binder molecules to the surface of silica/silicon. This is shown in **Figure** 2.

Building on these concepts, the work of Lu Zhang has demonstrated that similar reactivity can be optimized and built into the PAA binder system presently used. In the case of PAA, the slurry used by the CAMP team was optimized for viscosity, electrochemical activity, and laminate quality and is approximated as LiPAA. In Lu Zhangs study, he has assessed the pH stability of PAA between the two endmembers, Li[PAA] and H[PAA]. In the case of the surface reactivity, as noted by Neale and John Zhang, the opportunity to build in a leaving group by reaction of the surface with a proton is a desirable feature.   In the case of the PAA system, the protons have been eliminated at the lithium concentration and pH conditions used by CAMP in exchange for better electrode quality. Lu Zhangs work sought to recreate the desired viscosity of the slurry but retain the some of the protons used to build better Si-O surface bonds.   Their work has shown that more protons can be kept in the system if replaced in solution by an ammonia molecule that is eventually removed on annealing the laminate under normal processing conditions. The advantage of better viscosity is maintained by the pH adjustment but the reactivity is increased.

This work leads to the efforts by Armstrong and Veith on the role of surface aging and reactivity as it can be characterized by the use of system zeta potential. In this case several silicon's known to have high surface
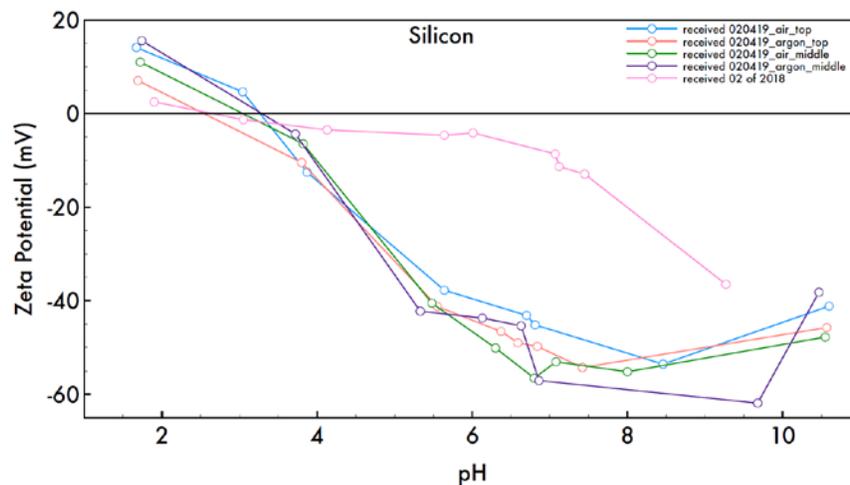

Figure 3: Zeta potential as a function of pH for silicon samples opened and tested in February 2019 where sampling was performed in: (1) air at the top of the bottle (blue), (2) argon at the top of the bottle (red), (3) air in the middle of the bottle (green), and argon in the middle of the bottle (purple). February 2018 (pink) was exposed to air. The black line represents the isoelectric point.

reactivity (see calorimetry studies by Allcorn, et al., (Sandia), testing studies by W, Lu (ANL), and NMR studies by Key (ANL) in previous reports; samples termed "February 2018" or "February 2019") were used to evaluate the aging phenomena of silicon surfaces. In these key studies, the aging of silicon in air or under argon was significant. Analysis showed that these reactive samples showed significant changes that would have an impact on the ability of the PAA binder to bind to the surface of the silicon. They have identified a pH range near pH=6 as the range that should be sought, a similar range that Lu Zhangs effort has found to be optimal for electrochemical performance of silicon electrodes with pH stabilized PAA binders. The discovery of the surface instabilities and use of dispersants to further equilibrate the silicon colloidal suspensions has opened up a new avenue of collaborative effort within the program that, when combined with Lu Zhangs pH-PAA optimization and Neale and John Zhangs surface functionality efforts should yield better quality electrodes when combined.

Composite Silicon / Graphite Electrodes

Variable Temperature Performance of Silicon-Gr Composite Electrodes (ANL)

María José Piernas, Ira Bloom, Alison Dunlop, S. Trask, A. Jansen

Background

Silicon is considered as a promising anode material to replace graphite in Li-ion batteries for electric vehicle (EV) applications, given the high capacity and, hence, the high energy density of this material. However, one factor that hugely affects the battery performance and that should not be overlooked, especially considering its ultimate goal, is the temperature at which an EV operates. To the best of our knowledge, the effect that temperature has on the cyclability of silicon has not been studied in depth. In this project, we are exploring the effect of temperature on the electrochemical performance of silicon anodes.

With this purpose, we studied four different material/electrolyte systems: silicon (Si) in Gen 2 (1.2 M $LiPF_6$ in EC: EMC, 3:7 wt%) electrolyte with and without 10 wt% of fluoroethylene carbonate (FEC), and silicon-graphite (Si-Gr) in Gen 2 with and without 10 wt% FEC.

Results

In the last report, we discussed the data obtained from Si-Gr half-cells cycled in Gen 2 electrolyte. In this quarter, we have focused on the results obtained from Si-Gr cycled in Gen 2 + 10 wt% FEC and how these compare with the former system.

Figure 4 displays how the capacity of Si-Gr electrodes varies as a function of cycle count and temperature applied. In absence of FEC, temperature affects the cyclability (**Fig. 4a**) of the material as well as its capacity (inset, **Fig. 4a**). As the Fig. 1a inset shows, the higher the cycling temperature, the larger the capacity achieved and the slower the effective C-rate (or time necessary to complete the charge). However, the cycle-life trend follows the opposite direction and the capacity fade rate is faster when the temperature increases. Conversely, the electrochemistry of Si-Gr seems to remain unaltered in presence of FEC, where similar capacity fade profiles (**Fig. 4b**) and capacities are observed (inset, **Fig. 4b**) regardless of the temperature applied.
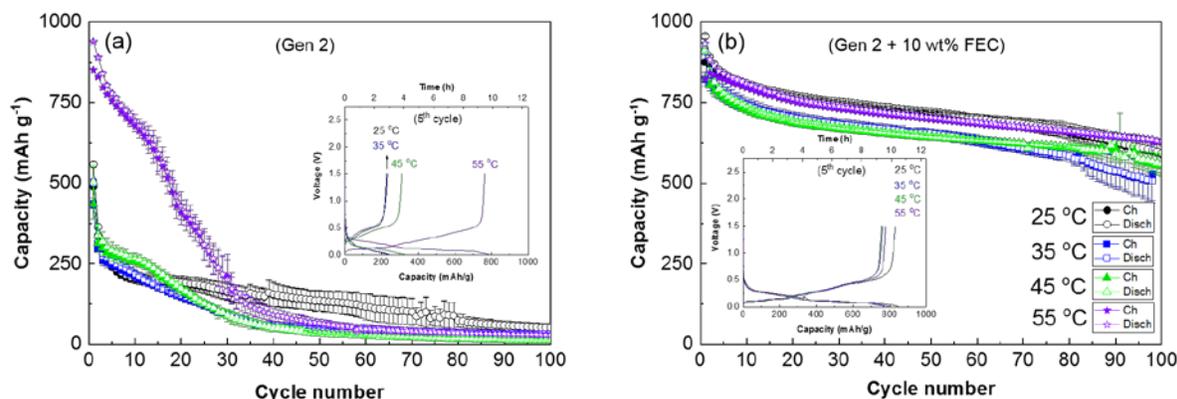

Figure 4. Charge and discharge capacity *vs.* cycle number plot of Si-Gr half-cells cycled at 25 (black), 35 (blue), 45 (green) and 55 ˚C (violet) containing Gen 2 electrolyte without FEC (**a**) and with 10 wt. % FEC (**b**). The filled and empty markers represent, respectively, the charge and discharge capacities. In all the cases, the Si-Gr electrodes were from CAMP (A-A013). Insets shows capacity obtained within the 5th cycle.

In order to find a possible explanation to the above-presented results, we ran HPPC tests (10 s 1C charge/discharge pulses, with 40 s rest in between). As expected, resistance changes with the temperature when Gen 2 is the electrolyte used (**Fig. 5a**). Since the cells investigated at 25 and 35 °C could not complete the HPPC protocol because they reached the upper upper limit voltage before 10% of delithiation during the 6th pulse, we were forced to compare the resistance values at 40 – 50 % SOC (state of charge). Within this SOC, the highest resistance was observed at 25°C; values approximately half of that were seen in the cells cycled at 35 and 45 °C, while the lowest resistance is detected at 55 °C. Interestingly, the addition of 10 wt% of FEC to the electrolyte drastically reduces the resistance, as illustrates **Fig. 5b**. Besides, the resistance values remain practically unchanged and seem to be independent of the temperature applied, which is consistent with the data displayed in Fig. 4b.
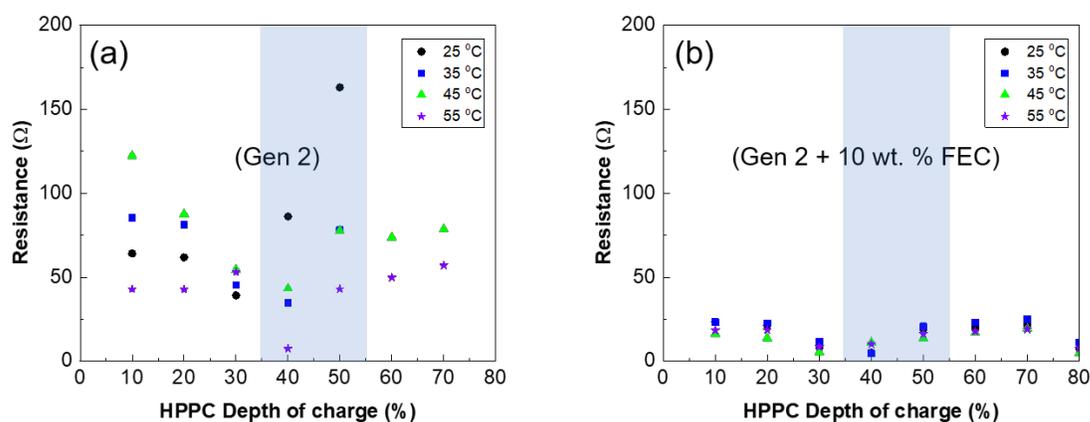

Figure 5. HPPC performance in the 5th delithiation of Si-Gr vs. Li+/Li in (a) Gen 2, (b) Gen 2 + 10 wt% FEC, at the different temperatures evaluated.

To further investigate the effect of temperature and the occurrence of possible different reaction mechanisms in cells tested without FEC, we are currently characterizing cycled Si-Gr electrodes by several techniques (XRD, GC-MS, FTIR, SEM).

Conclusions

The electrochemical performance of Si/Gr half-cells have proved to be temperature-sensitive when the material is cycled using Gen 2, whereas they are temperature-non-sensitive when FEC is added to the electrolyte mixture. The main reason behind such a distinct behavior has been related to changes in the cell resistance. Therefore, the role of FEC is definitely crucial for high-temperature cycling.

Presentations

1) M. J. Piernas-Muñoz, S. E. Trask, A. R. Dunlop and I. Bloom "Effect of temperature on silicon-based anodes for Li-ion batteries" *J. Power Sources* 2019 (submitted).

2) M. J. Piernas-Muñoz, A. Dunlop, S. E. Trask, I. Bloom. "Temperature Influence on Si-based Anodes for Li-ion batteries" International Battery Association 2019 (IBA 2019). March 3-8, 2018. UC-San Diego, La Jolla, California, (USA).

Silicon – Containing Anodes with Extended Cycle Life and Calendar Life (PNNL)

Ji-Guang Zhang, Xiaolin Li

Nanoscale silicon, a highly porous structured silicon material, has been widely used as a stable silicon electrode component in an effort to avoid pulverization of silicon particles during cycling process. However, the large surface area of nanosilicon or micron sized porous silicon also has been noted to lead to a continuous reaction between lithiated silicon and electrolyte, with evidence of gassing or electrode degradation reported. As a result of these reactions, continuous growth of SEI layer and increase of cell impedance have been noted. Another possible degradation mechanism is cross-talk within the cell between silicon anode and cathode. This event, for example dissolution of Mn from the surface of an NMC or spinel cathode followed by cation transport to the anode side, can poison the anode SEI. The addition of FEC as an additive has been shown to form an effective and stable SEI layer on silicon but may also form a electrolyte-based film at the cathode interface (CEI) leading to an impedance increase. Our goal is to minimize the surface area of silicon and find a stable electrolyte additive are critical for long term stability of silicon based Li-ion batteries.

In this project, we seek to enhance the cycle life and calendar life of silicon-based Li-ion batteries by creating a stable porous silicon structure in conjunction with an artificial SEI layer coating. In association with these objectives, a more stable electrolyte additive or solvent mixture will be investigated to minimize the effect of FEC at the cathode interface. The degradation mechanism of silicon anodes during shelf storage will be systematically investigated. New insights on these mechanisms and the new approaches developed in this work will speed up the deployment of high energy Li-ion battery with silicon-based anodes and increase market penetration of EVs and PHEVs, which supports DOE's mission for energy efficiency and affordability.

Results

In last quarter, LiFSI-based localized high concentration electrolytes (LHCEs) with EC-EMC have been developed for the Si anodes made by ANL/CAMP facility. Electrolytes with different salt concentration were screened and the results demonstrated that E-104 with the salt concentration of 1.8M enables the best performance in terms of specific capacity (114.8 mAh/g vs. 96.3 mAh/g for Gen II electrolyte in 4th cycle,), FCE (75% vs. 60% for Gen II electrolyte) and cycling stability (92.4% vs. 55% for Gen II electrolyte in 100 cycles). The testing results also revealed that the molar ratio of the solvent and diluent has an optimized value for the best performance. In this quarter, the NMC532|| Si/Gr cells with E-104 demonstrated superior long-term cycling performance with the capacity retention of 81.8% after 200 cycles (**Figure** 6a). In addition, we also verified the high voltage stability of E-104 versus NMC cathode in NMC532|| Li cells. These cells show stable cycling up to 4.5 V with E-104 electrolyte, while exhibits quick capacity fading when they were charged to > 4.3 V in baseline electrolyte (**Figure** 6b). These results clearly indicated that NMC532|| Si/Gr cells using E-104 can be charged to higher voltage to obtain higher energy densities.

Furthermore, the effects of the electrolytes on the end-of-life (EOL) swelling of electrode were also evaluated and compared. Table 1 shows the thickness of Si/graphite composite electrodes before testing and after 100th cycle at full de-lithiation condition. The average thickness of the pristine electrode was 28μm, while the average electrode thickness at 100th was 52 μm in E-baseline (Gen II electrolyte), 42 μm in E-101, 42 in E-102, 40 μm in E-104, and 46 μm in E-106. Thus, the EOL swelling of electrode was 85.7% in baseline electrolyte, 50% in E-101, 50% in E-102, 42.8% in E-104 and 64.2% in E-106. It is demonstrated that the E-104 can greatly suppress the EOL swelling of the Si-based electrodes, which is critical to the maintenance of the Si electrode structure and the stability of the Si electrode and the cell during cycling.
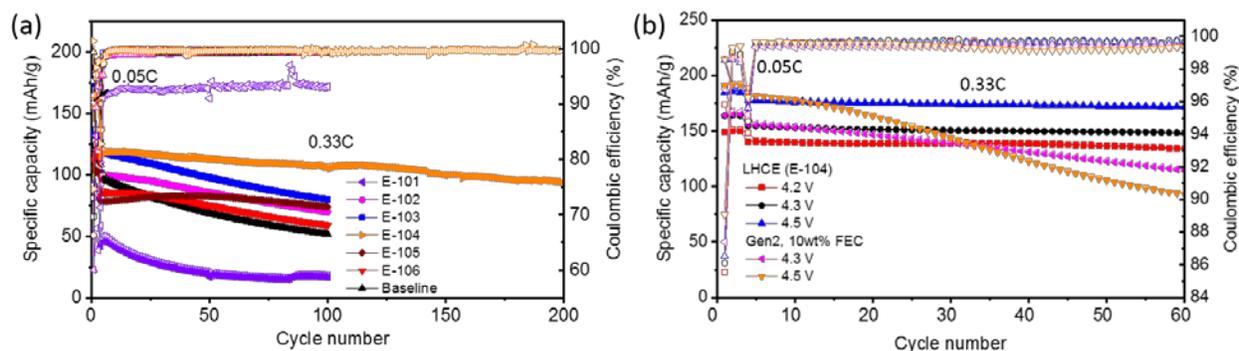
Figure 6. a) Cycling performance of NMC532|| Si/Gr (CAMP electrodes) in BTFE-based electrolytes with different salt concentration; b) high voltage stability of NMC532|| Li in E-104 and baseline electrolytes.

Table 1. The swelling of Si/Gr anode in different electrolytes

	Pristine Si anode thickness (μm)	Thickness of de-lithiated Si anode (μm) at 100th cycle	Swelling at 100th cycle
E-baseline	28	52	85.7%
E-101	28	42	50%
E-102	28	42	50%
E-104	28	40	42.8%
E-106	28	46	64.2%

The electrochemical impedances (EIS) of NMC532|| Si/Gr cells at different cycles were measured and further analyzed by the distribution of relaxation time (DRT). As shown in **Figure** 7a, the cell resistances after first cycle are in the order of E-101> E-102> E-control>E-103=E-104> E-105. After 50 cycles, the cell resistance in descending order is E-control>E-101>E-105>E-103=E-106>E-102>E-104 (**Figure** 7b), which is consistent with the electrochemical performance results. DRT analysis is an effective method in unveiling the emergence of new electrochemical processes (i.e. new SEI/CEI and charge-transfer at the evolving interface) upon cycling, which is often concealed or ambiguously de-convoluted by the complex EIS spectra. It was calculated from the obtained impedance spectra to make a clearer separation of electrochemical process with different time constant. As shown in **Figure** 8, four distinct peaks are observed in the frequency range of 10^4 to 0.1 Hz (e.g. the relaxation time range of 10^{-4} to 1 s), which can be ascribed to Li^+ migration (R_{SEI}) in SEI and CEI (ca. 10^4-10^3 Hz) and corresponding charge-transfer processes of R_{ct} (ca. 10^2-0.1Hz). DRT analysis of the Si/Gr||NMC333 full cell using baseline electrolyte showed a substantial increase in the second peak of R_{ct} and general higher R_{ct} compared to that obtained in LHCEs. DRT analysis of the full cell using E-106 exhibited an increase in both peaks of R_{SEI} and higher Rct compared to E-104 at 50th cycle which means the transport of Li^+ becomes slower when the molar ratio of BTFE to solvent reaches 3. This is probably because more Li^+ was trapped in FSI cluster as BTFE increases. DRT analysis of the full cell using E-104 showed a decrease in the first R_{ct} and smaller R_{SEI} compared to E-101 and E-106, which indicates E-104 can well protect both cathode and anode, thus resulting in remarkable improvement of cycling performance and suppression of structure swelling of Si anodes.
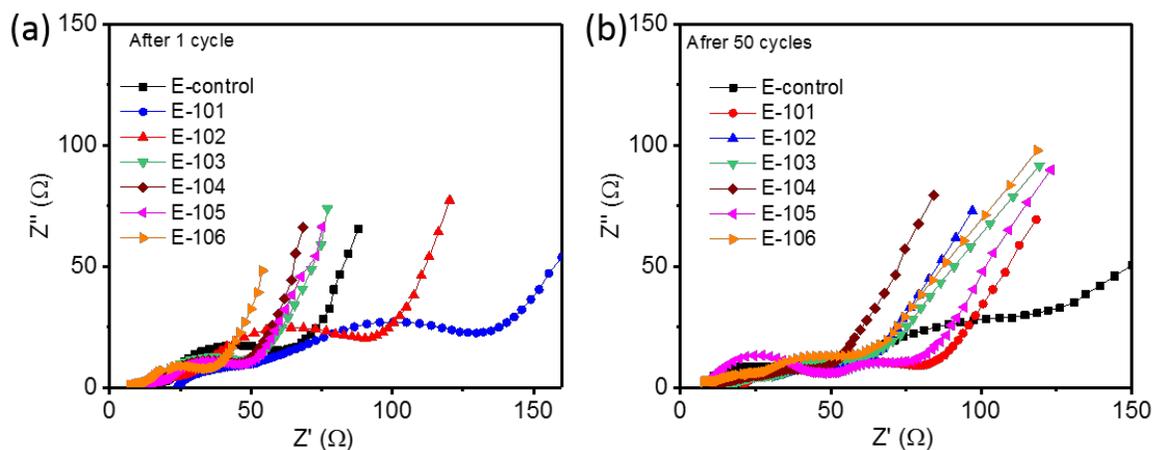
Figure 7. Nyquist plots of Si/Gr||NMC532 full cells with different electrolytes obtained in different cycles.
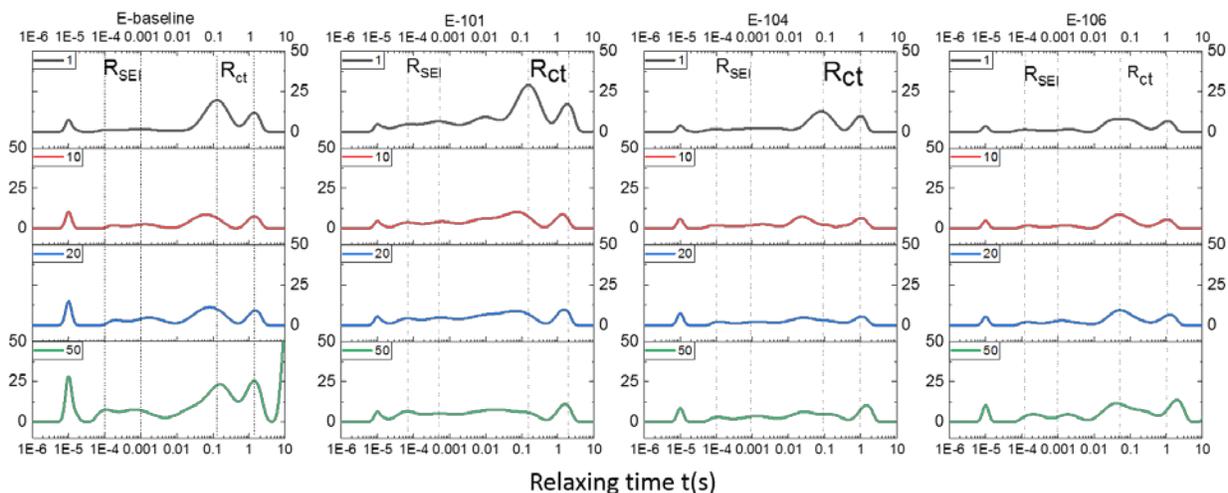

Figure 8. DRT analysis for corresponding impedance spectra of the Si/Gr||NMC532 full cells with different electrolytes obtained in different cycles.

Conclusions

For deep dive anodes with LiPAA binder, LHCE with controlled overall salt concentration of 1.8M enables the best performance in terms of specific capacity, cycle life and electrode swelling. The characterization results further demonstrate that there is an optimized diluent amount for localized high concentrated electrolytes to enable the best electrochemical performance of silicon anodes.

Dynamic Surface Chemistry of Silicon Electrode Materials (ORNL)

Katie Burdette (ORNL), Beth Armstrong (ORNL), Alex Rogers (ORNL), Andrew Jansen (ANL), Bryant Polzin (ANL) and Gabriel Veith (ORNL)

Background

Because all silicon materials are not created equal, the zeta potential and particle size of Vendor Sample 4 nanosilicon (Lot #F17-021-LS) as a function of aging was investigated. It is believed that the surface of the material is changing as a function of age; therefore, it is imperative to confirm this hypothesis and understand these changes in order to produce uniform electrodes. In this work, the surface of the reactive silicon material obtained and opened in February 2018 was compared with an identical, *but unopened or annealed,* bottle of the same material opened in February 2019. Due to the variability of the bottle opened in 2018, there was some suspicion that the Si at the top of the bottle may differ from that at the middle of the bottle. Therefore, a systematic study of Si as a function of depth in bottle was also performed. We found large variability in zeta potential (>40 mV) and particle size with the age of the material as well as the sampling depth of the Si.

Results

The surface chemistry of the electrode material will dictate electrode formation processes, polymer interactions and we suspect SEI formation. The most effective tool to characterize the surface is through measuring the zeta potential. Zeta potential is a measure of the electrical potential between the first tightly bound solvent shell
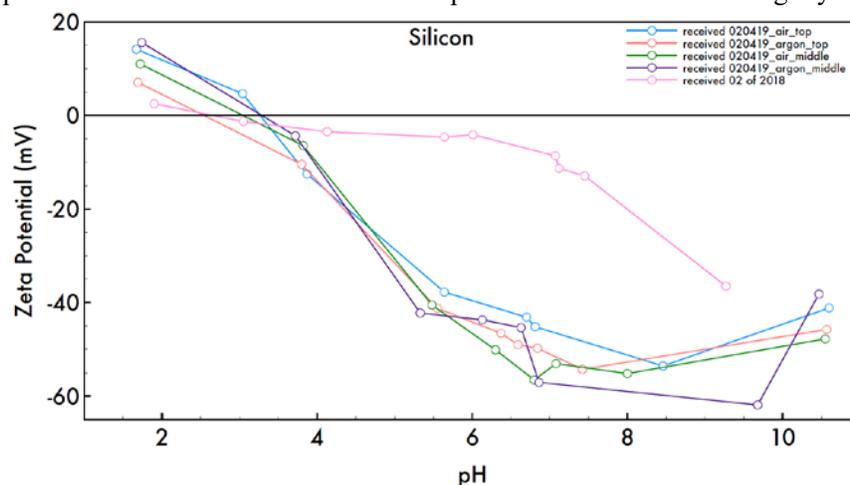

Figure 9: Zeta potential as a function of pH for silicon samples opened and tested in February 2019 where sampling was performed in: (1) air at the top of the bottle (blue), (2) argon at the top of the bottle (red), (3) air in the middle of the bottle (green), and argon in the middle of the bottle (purple). February 2018 (pink) was exposed to air. The black line represents the isoelectric point.

(called the Stern layer) and the second solvent shell (diffuse layer). The particle moves when the Stern layer slips by the diffuse layer. Voltage needed to induce slipping is the measured zeta potential, which is a calculated value. Another way to look at zeta potential is as a measure of electrostatic stability in a dispersion where the absolute value of 30 or greater is considered colloidally stable.[1] Each zeta potential curve presented herein is the calculated zeta potential as a function of pH, which show the pH/stability/dispersability relationship, which is important in understanding the role of the Si surface in electrode architecture.

The pink curve in **Figure** 9 shows the zeta potential measured in February 2018. Notice that the material does not become electrostatically stable until a pH of ca. 9 is reached. For reference, a pH of 5-6 is the working range for slurry production and electrode fabrication. However, silicon from the same lot number, but unopened, was tested in February 2019 showed electrostatic stability at a pH of ca. 4.5. Within the working pH range, the

February 2018 sample maintained a zeta potential of approximately -7 mV (colloidally unstable), while the February 2019 material showed a zeta potential of approximately -50 mV (colloidally stable). This is significantly different and points to manufacturing issues or significant aging issues.

To explore these differences further the February 2019 bottles were split up to store them in an argon filled glove box or in air. Furthermore, samples from the top of these bottles and bottom of these bottles were investigated to explore differences as a function of depth from the top (closest to air) of the bottles. While the zeta potential
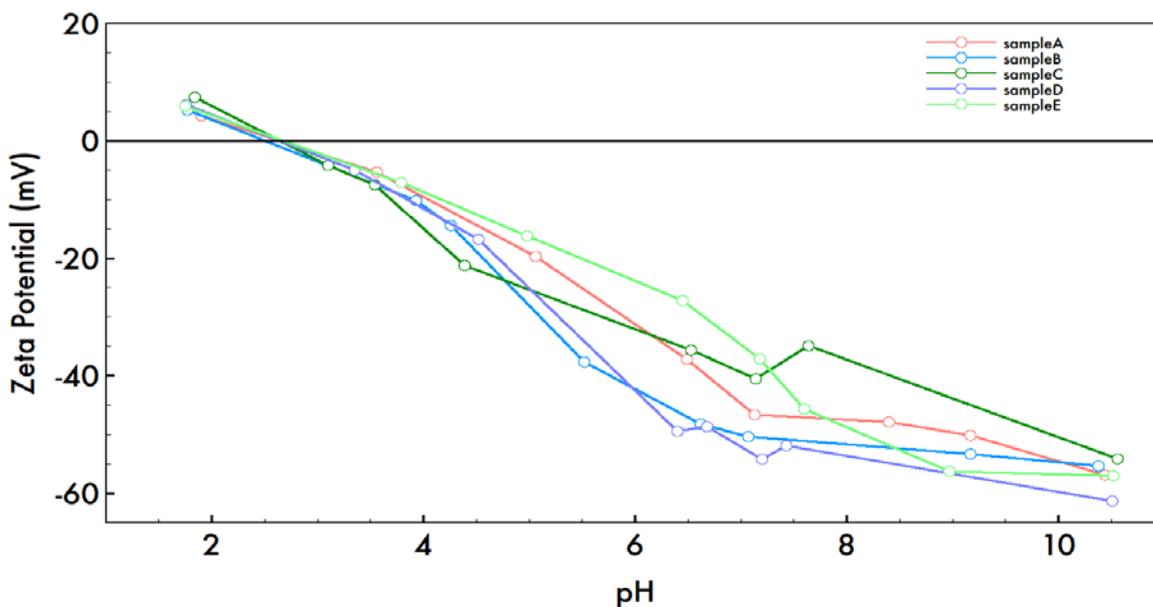

Figure 10: Zeta potential versus pH for ORNL silicon milled with various polymers. Each curve represents silicon from the same feedstock being ball milled with a different polymer. Black line is the isoelectric point line.

for all materials tested in February 2019 trended with the same general potential curves, the isoelectric point varied greatly within the batch (pH range 2.5-3.5), which suggests that the surface of the silicon within the same batch is not the same (*cf.* **Figure** 11). Indeed, the isoelectric point, i.e. the point at which there are no repulsive forces in the dispersion yielding a zeta potential of zero, for these materials varies by more than 1 pH point, indicating that there are differences in the Si surfaces as a function of position within the batch. This is a significant variation for this technique. To ensure that this observed difference was statistically accurate, ORNL silicon was ball milled with various polymers, and the powders were characterized using zeta potential. Even though these silicon materials were milled with different polymers, their isoelectric point does not vary by more than a few percentage points, indicating that the isoelectric points observed with the silicon samples are significant (*cf.* **Figure** 10).

To investigate the possible difference between the surfaces of the silicons tested in February 2018 versus February 2019, we studied heat-treated silicon from the same lot. It was found that the silicon heat treated at 400ºC in air produced the most consistent zeta potential results when compared with the material tested in February 2019. Heat treatment in air will produce more SiO_2 species on the surface, which we hypothesized to material left at atmospheric conditions over a long period of time (i.e. over one year).[2] Additionally having a more uniform oxide surface will electrostatically stabilize the particles more than having a mixture of oxide and hydride species

as silicon is generally covered with hydride species before it oxidizes.[3] Therefore, it was hypothesized that the material opened in February 2018 may have a larger variety of species on its surface while the material opened February 2019 was more fully oxidized.[4] The Si from February 2018 versus February 2019 also showed a large
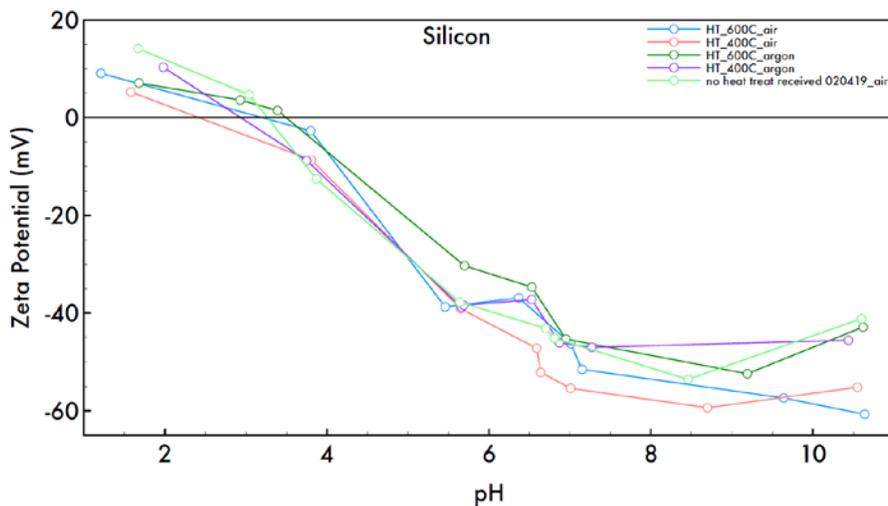

Figure 11 Zeta potential as a function of pH for silicon that was heat treated in air at 600°C (blue) or 400°C (red) or in argon at 600°C (dark green) or 400°C (purple). Zeta potential as a function of pH for2019 silicon exposed only to a laboratory atmosphere (light green) is provided for reference. Black line is the isoelectric point line. All materials were tested in February 2019.

difference in average particle size as a function of pH. Material tested in 2018 showed a particle size of about 500 nm with a slightly smaller average size in the pH 7.5-9.5 regime, while in the pH range 5.5-10 material opened in 2019 showed a particle size of about 300 nm and at low pH's particles were evident in the 1 μm range (*cf.* **Figure** 12). This trend was also observed for the heat-treated silicon in air and in argon indicating that oxide formation promotes agglomeration at highly acidic conditions, but that oxide formation yields smaller particles within our working range (pH 5-6) and at basic conditions (*cf.* **Figure** 13). Smaller particles tend to lend themselves to making more uniform electrodes
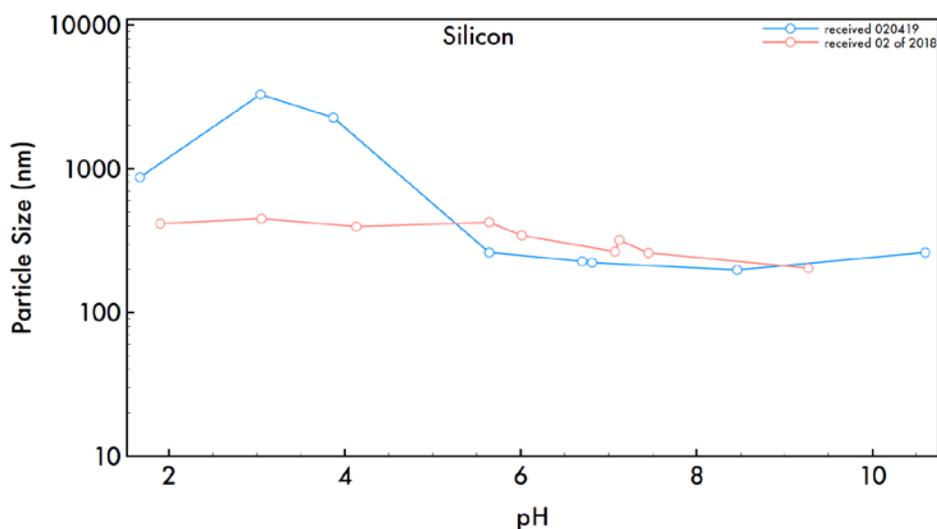

Figure 12 Particle size as a function of pH for (top) 2019 silicon in air (blue) and February 2018 (red)
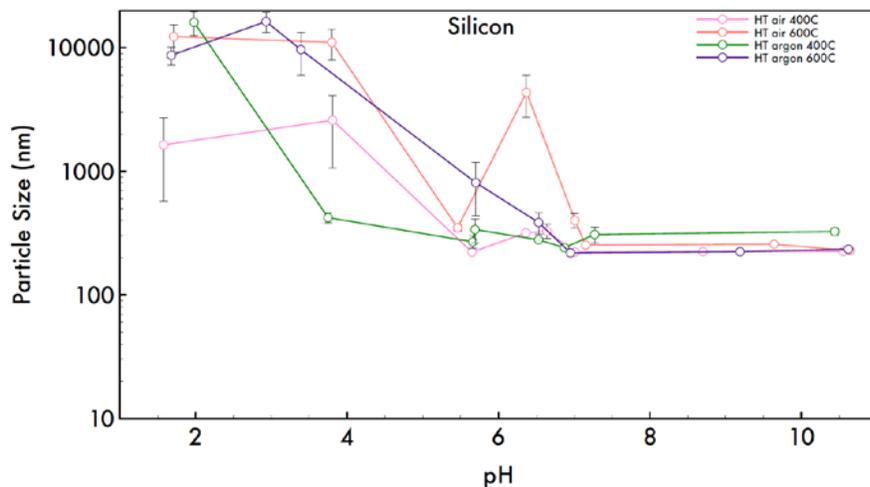
Figure 13: Particle size of silicon heat treated in (1) air at 400ºC (pink), air at 600ºC (red), argon at 400ºC (green), and argon at 600ºC (purple).

Conclusion

This data shows the power of time resolved zeta potential and light scattering measurements. Clearly there are changes in the surface chemistry and particle sizes of the silicon with age and exposure to air or dry argon. This data indicates that the age of the silicon material plays an important role in its surface chemistry or there are reproducibility issues with silicon manufacturing and these un-annealed samples. The material can potentially be made more electrostatically stable with aging. Aging seems to promote SiO_2 growth, which yields more dispersable particles as well as smaller particles within the working range of the slurry and electrode cast. It will be important to note the age of the silicon material or develop controlled processing measures to impart a known surface to the silicon. The uncontrolled agglomeration of Si particles will not lend itself to the formation of uniform electrodes with controlled architecture. Further characterization of this relationship with electrochemical performance is required.

References

1) Bhattacharjee, S., "DLS and zeta potential - What they are and what they are not?" *Journal of Controlled Release* **2016,** *235*, 337-351.

2) Engel, T., "The Interaction of Molecular and Artomic Oxygen with SI(100) and SI(111)". *Surface Science Reports* **1993,** *18* (4), 91-144.

3) Waltenburg, H. N.; Yates, J. T., "Surface Chemistru of Silicon". *Chemical Reviews* **1995,** *95* (5), 1589-1673.

4) Zhuravlev, L. T., "The surface chemistry of amorphous silica. Zhuravlev model" *Colloids and Surfaces a-Physicochemical and Engineering Aspects* **2000,** *173* (1-3), 1-38.

Binders and Surfaces for Composite Silicon Electrodes (ANL)

Zhangxing Shi, Sisi Jiang, and Lu Zhang (Argonne National Laboratory)

Background

The conventional Li-intercalation electrode material, graphite, has relatively low gravimetric (0.37 Ah/g) and volumetric (0.89 Ah/cm^3) capacity that cannot meet the ever-growing power demand. Silicon (Si) emerged as a Li-alloying electrode material due to its low cost and high theoretical gravimetric (4.2 Ah/g) and volumetric (2.4 Ah/cm^3) capacity. However, commercial use of Si-based negative electrodes has been hindered by its large volumetric expansion (~320%) along with Li alloying, which leads to unstable solid-electrolyte interphase (SEI), rapid loss of cohesion in the electrode matrix, and particle pulverization. Compatible polymer binders including alginate, carboxymethyl cellulose, poly(vinyl alcohol) and poly(acrylic acid) (PAA) have been utilized to mitigate these problems. These binder materials could provide strong adhesion between the active materials (graphite and/or Si) and conductive carbon particles, keeping them in electric contact despite the large volume changes of Si particles during electrochemical cycling. Among the reported binders, PAA has been selected as the standard binder material for the Silicon Deep Dive program. However, the factors affecting the performance of PAA binders are not fully understood and the performance of silicon lithium-ion batteries using PAA based binders is still far from meeting the requirement of practical use. Therefore, it is important to gain in-depth understanding of the performance of PAA based binders and evolving those binders towards desired cell performance for silicon lithium-ion batteries.

Lithiation of PAA binders is a common strategy for silicon lithium-ion batteries, which could benefit the large-scale lamination process and enable the fabrication of mechanically robust electrodes. The viscosity of PAA solution increases significantly by lithiation that could potentially improve the slurry stability. However, the same process also involves a strong base, lithium hydroxide or LiOH, which dramatically impacts the pH values of PAA solutions. These variations consequently lead to property changes of the pH-responsive PAA binders, affecting Si chemical stability and cell performance. An ideal case would be enhancing the viscosity of the binder solution to improve the slurry stability with no or minimum pH increase. Three approaches have been proposed to study high performance binders for silicon lithium-ion batteries. **Firstly**, instead of LiOH, non-lithium bases, such as NBu$_4$OH and NH$_4$OH (Et$_3$N) were used to tune the viscosity of PAA solutions. **Secondly**, the solvation behavior and viscosity of PAA binders in various solvents have been investigated by ultra small-angle X-ray scattering (USAXS) and rheometry. The fabricated electrodes using these binder/solvent systems were evaluated in silicon half cells. **Thirdly**, modified PAA derivatives (e.g., poly(maleic acid), poly(vinyl alcohol-alt-maleic acid), poly(tartronic acrylate), and poly(citric acrylate)) have been pursued as new binder materials.

Results

Compared to aqueous PAA solution, lithiated PAA solutions with the same wt% in water have significantly improved viscosity at low shear rate and better shear thinning effect. Preliminary studies on the relationship between binder viscosity and slurry stability showed that lithiated PAA binders could improve the stability of the slurry due to its high viscosity. For example, two slurries containing the same amount of electrode materials were made using straight PAA and PAA with 85% lithiation (i.e., PAA-85%Li) binders, respectively. After sitting in sealed container for 12 h, the PAA-85%Li slurry still looks the same while the straight PAA slurry becomes too and is not suitable for lamination anymore. For PAA-85%Li solution, since it has much higher viscosity than straight PAA solution, it requires more water added to the slurry to achieve the desired state for lamination. For instance, to make slurries consist of 1.00 g graphite, 0.205 g Si, 1.37 g binder solution, and 0.027 g C45, 0.514 g extra water was added for straight PAA slurry while 1.527 g extra water was added for PAA-85%Li slurry. The water added to the PAA-85%Li slurry is three times of that of straight PAA slurry, therefore the PAA-85%Li slurry could be more stable due to better dispersion of electrode materials and less impact of

water evaporation. On the other hand, according to our previous studies, lithiated PAA binders suffer more capacity loss in both half cells and full cells because of the increased pH value of the binder solution. To investigate the balance between slurry stability and cell performance, PAA solutions (M_n = 147 kDa, PDI = 4.9) modified by mixing with non-lithium bases, such as NBu$_4$OH (PAA-TBA), Et$_3$N (PAA-TEA), and NH$_4$OH (PAA-NH$_3$) were prepared. Those bases are supposed to tune the viscosity the same way as LiOH but with less
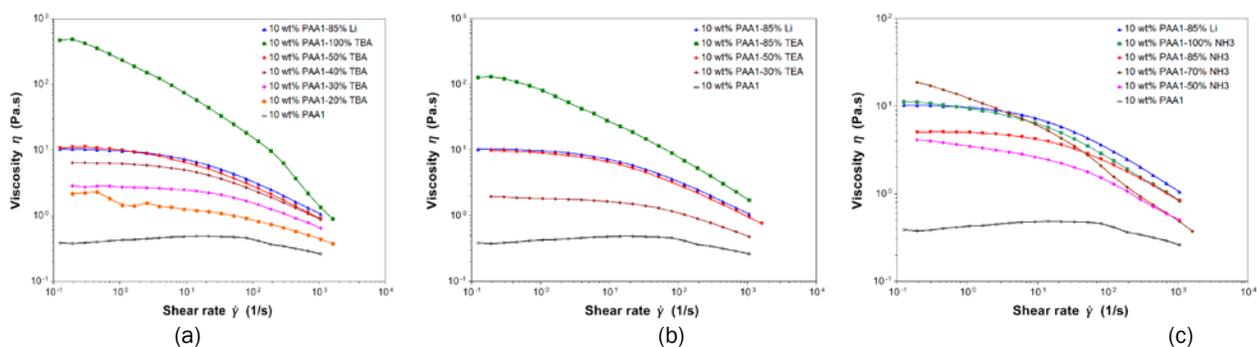

Figure 14. Plots of apparent viscosity vs. shear rate for 10 wt% aqueous solutions of (a) PAA mixed with NBu$_4$OH, (b) PAA mixed with Et$_3$N, and (c) PAA mixed with NH$_4$OH. PAA and PAA-85%Li were chosen as two baselines for comparison.

impact on pH increase. The apparent viscosity vs. shear rate of these modified PAA solutions were measured by TA Discovery HR-2 Rheometer (see **Figure 14**). As shown in **Figure 14a**, PAA-TBA solutions showed significantly higher viscosity compared to straight PAA solution. Notably, PAA-TBA solution mixed with only 50% of NBu$_4$OH achieved similar viscosity and shear thinning as PAA-85%Li solution. Since less base was needed to achieve the desired viscosity, the pH of PAA-50%TBA solution (pH = 5) is lower than PAA-85%Li solution (pH = 6). PAA-TEA solutions showed promising viscosity improvements similar to PAA-TBA solutions (**Figure 14b**). The pH values of PAA-TEA solutions are even lower because triethylamine is a weak
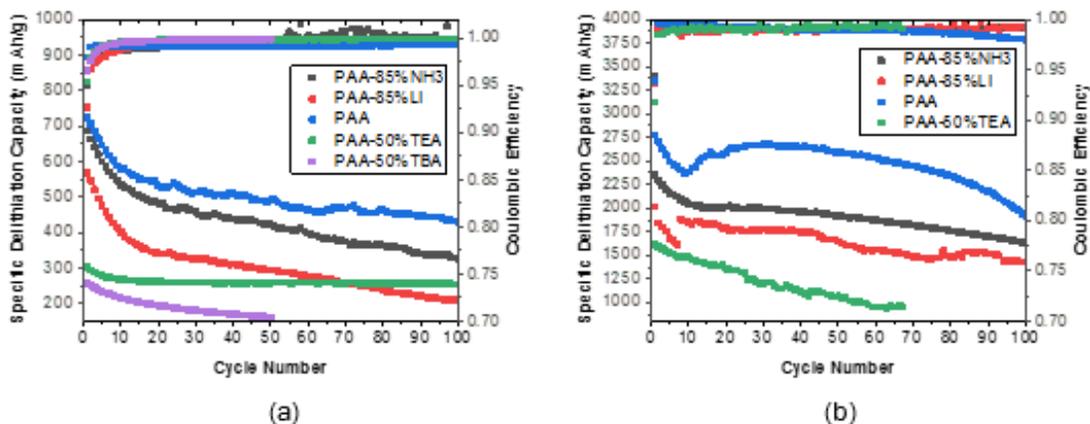

Figure 15. (a) Specific delithiation capacity profiles (to the left) and coulombic efficiency profiles (to the right) of half cells using electrodes contain 73 wt% graphite, 15 wt% Si, 10 wt% modified PAA binders, and 2 wt% C45 over 100 cycles at C/3 rate; (b) Specific delithiation capacity profiles (to the left) and coulombic efficiency profiles (to the right) of half cells using electrodes contain 70 wt% Si, 20 wt% modified PAA binders, and 10 wt% C45 over 100 cycles at C/3 rate.

base (e.g., pH of PAA-50%TEA = 4.5). The viscosity data of PAA-NH$_3$ solutions is comparable with PAA-85%Li solution (**Figure 14c**), while the pH of PAA-85%NH$_3$ solution is much lower (pH = 5) as NH$_3$ is also a weak base. Moreover, NH$_3$ only acts as a temporary additive during the lamination process to boost viscosity and could be removed by thermal decomposition during the drying process. The capacity profiles of graphite-Si composite (15wt% Si) electrodes and all Si (70wt% Si) electrodes made with these modified PAA binders were

summarized in **Figure 15**. When using PAA-50%TBA as binder, cells have very low initial capacity (ca. 255 mAh/g), even lower than theoretical graphite capacity. Cells using PAA-50%TEA binder also showed low initial capacity for both composite electrode (ca. 303 mAh/g) and all Si electrode (ca. 1756 mAh/g). These low capacities indicated that PAA-50%TBA and PAA-50%TEA are not suitable binder materials possibly due to the overly large ammonium cations that could interfering with the binding interactions. However, PAA-85%NH$_3$ showed promising capacity profiles. As shown in **Figure 15a**, cells with PAA-85%NH$_3$ binder have higher initial capacity (ca. 686 mAh/g) and capacity retention than those of PAA-85%Li cells (569 mAh/g). Similar results were also observed for high content Si cells (initial capacity = 2348 mAh/g for PAA-85%NH$_3$ cells and initial capacity = 2017 mAh/g for PAA-85%Li cells), as shown in **Figure 15b**. While the performance of PAA-85%NH$_3$ binder is not as good as straight PAA, the increased viscosity of PAA-85%NH$_3$ solution could help improving the stability of the lamination slurry. Father investigations regarding tuning viscosities of binder solutions are ongoing to pursue optimized balance of the slurry stability and cycling performance.

Understanding the solvation behaviors of PAA based binder solutions can be very useful to better tuning the properties of binders and further optimize the balance of the slurry stability and cycling performance. A series
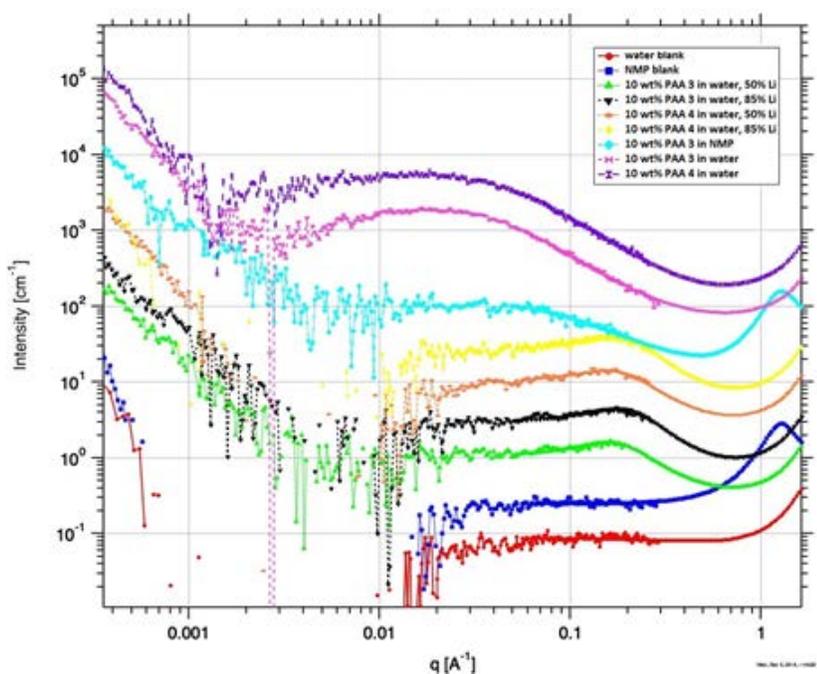

Figure 16. Ultra small angle X-Ray scattering (USAXS) profiles for PAA solutions

of 10 wt% PAA solutions were prepared under various conditions for USAXS analysis in collaboration with Jan Ilavsky (APS, Argonne National Laboratory) (**Figure 16**). The radius of gyration (Rg) was calculated by curve fitting of the broad peak in each profile. The results indicated that Rg values seem to be a good indicator for the cell performance as the high Rg, the better cell cycling results can be expected.   It is also observed that Rg was affected by polymer molecular weight, lithiation, and the choice of solvent. High molecular weight, non-lithiation, and water seem contribute to the higher values of Rg. While no other evidence has been shown, we speculate that the high Rg values may be associated with more inter connected conformations of the binders in solutions, which could be beneficial to adhesion and/or cohesion to the electrode matrix. In our previous studies, we have done some work trying to understand the relationship between molecular weight, or the lithiation of PAA binders, and their electrochemical performance. But the solvent impact on the binders and fabricated cells is still of little knowledge. To study this, several solvents or solvent combinations were chosen for the slurry making process based on certain properties (e.g., solvation of PAA, clustering of PAA). The evaluation of the electrodes fabricated based on those processing solvents are still ongoing.

At last, several PAA derivatives were designed and synthesized as new binder materials including poly(maleic acid) (PMA), poly(vinyl alcohol-alt-maleic acid) (PVA-alt-PMA), poly(tartronic acrylate) (PTA), and poly(citric acrylate) (PCA) (**Figure 17**). These new polymers have multiple carboxylic acid groups in each repeat unit which could improve the binding interactions between electrode materials. The characterization and cell evaluation of these
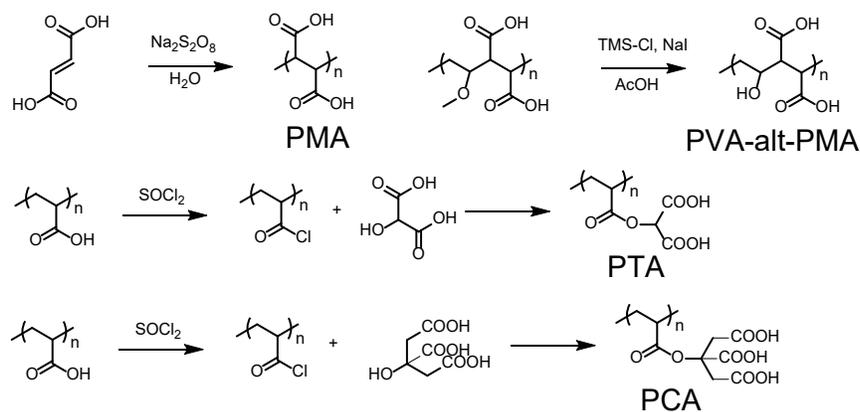

Figure 17. Synthetic scheme of PAA derivatives as new binder materials.

Conclusions

The balance between slurry stability and performance has been investigated by tuning the viscosity of PAA solution. Among the modified PAA binders, PAA-85%NH$_3$ showed promising viscosity results and cell performance for both graphite-Si composite electrodes and all Si electrodes in half cell tests. The solvation behavior of PAA binders was explored using USAXS analysis and composite electrodes fabricated with various PAA/solvent(s) combinations were evaluated in half cells. Several new PAA derivatives were designed and synthesized as new binder materials. These new polymers will be evaluated as binders in the near future.

References

1. Wu H.; Cui, Y. *Nano Today* **2012**, *7 (5)*, 414-429.
2. Hu B.; Shkrob I. A.; Zhang S.; Zhang L.; Zhang J.; Li Y.; Liao C.; Zhang Z.; Lu W.; Zhang L. *J. Power Sources* **2019**, *416*, 125-131.
3. Erogbogbo F.; Lin T.; Tucciarone P. M.; LaJoie K. M.; Lai L.; Patki G. D.; Prasad P. N.; Swihart M. T. *Nano Lett*. **2013**, *13(2)*, 451-456.

Next Generation Anodes for Lithium-Ion Batteries (LBNL)

Wei Tong (LBNL)

Background

Background

Thin films free of binder/conductive carbon additive offer the opportunity to enable the effective characterization of solid-electrolyte interphase (SEI) formation and evolution upon electrochemical cycling. In this quarter, using multi-target sputtering instrument, we moved forward from synthesis of individual Si and Sn films on smooth Cu foil substrate towards co-sputtering two separate Si and Sn targets to produce Si-Sn composite thin films with varied compositions. The ultimate goal is to identify promising Si-based thin film compositions as baseline and provide guidance for the synthesis of Si-based thin splats by splat quenching method. Structural and electrochemical properties of the as-produced films were investigated and discussed.

Results

Si-Sn composite thin films were directly deposited onto 12-µm-thick Cu foil by pulsed direct current (DC) magnetron co-sputtering using a 3-inch p-type Si target (Kurt J. Lesker, 99.999% purity) and a 3-inch Sn target (Kurt J. Lesker, 99.998-99.999% purity). The power level was varied between 25 and 200 W to tune the film
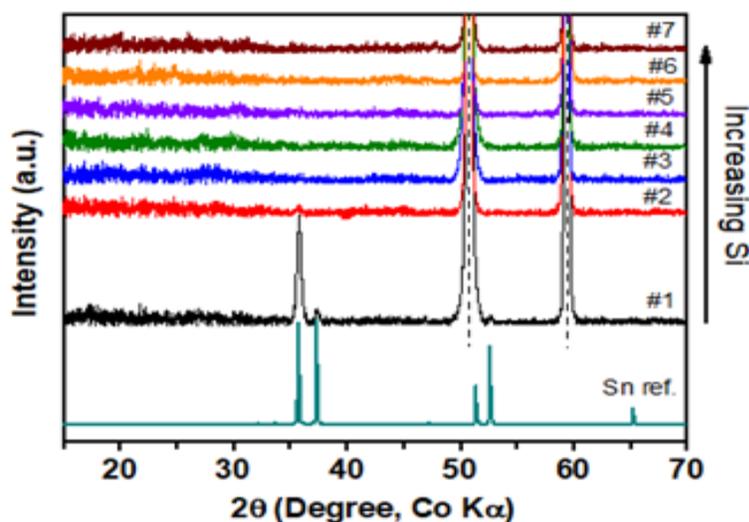

Figure 18. XRD patterns of Si-Sn films co-sputtered from separate Si and Sn targets. Dash lines mark Cu current collector.

composition. All the as-deposited films were subsequently stored under vacuum to prevent air exposure. 2032-type coin cells were assembled using the as-produced film (1.6 cm^2) directly as the working electrode, Li metal foil as the counter electrode, and 1.2 M LiPF$_6$ in ethylene carbonate (EC)-ethyl methyl carbonate (EMC) (3:7 by weight) as the electrolyte (Gen2). The cells were galvanostatically cycled between 1.5 and 0.01 V at C/20 based on the experimental capacity.

Figure 18 shows the X-ray diffraction (XRD) patterns of the co-sputtered Si-Sn thin films, along with the Sn reference, collected using Co Kα radiation. The Si content in the composites increases from Si-Sn sample #1 to #7. The film morphology and composition will be investigated by scanning electron microscopy (SEM) and

energy-dispersive X-ray spectroscopy (EDS). As shown in **Figure** 18a, except for the Si-Sn film with the lowest Si content (black line), characterized by crystalline Sn (c-Sn) peaks, other films are nearly X-ray amorphous. Note the two strong X-ray peaks around 50 and 60^0 are from Cu foil. Such X-ray amorphous feature is believed to avoid the two-phase formation during lithiation and delithiation, therefore, improved cycling performance is anticipated for the amorphous films. It's worth noting that Sn tends to crystallize even at room temperature as reported last quarter. We confirm that X-ray amorphous films can be obtained when co-sputtering Si and Sn when Si content reaches to a certain range.

Figure 2a-g show the voltage profiles of the as-produced Si-Sn thin films, from #1 to #7 with increasing Si
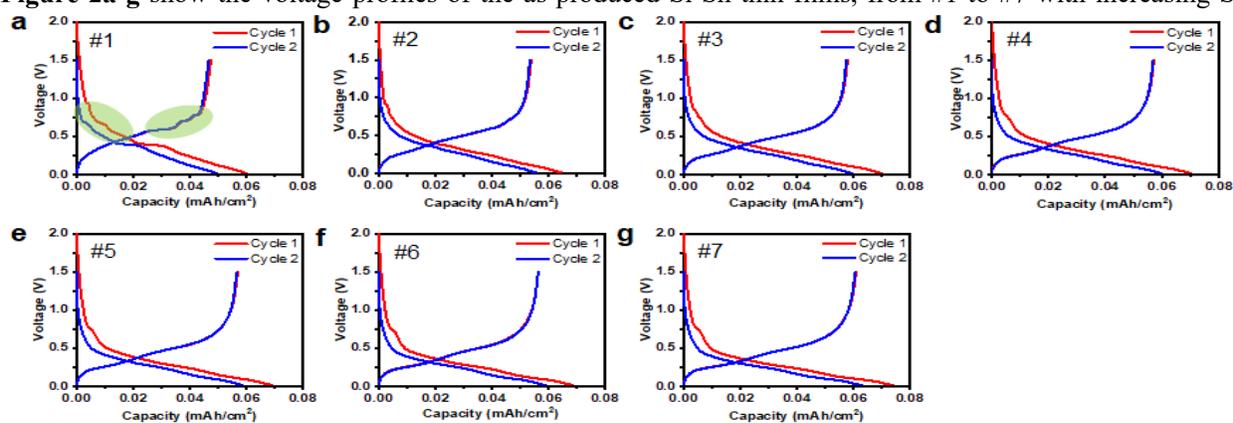

Figure 19. Voltage profiles of Si-Sn films co-sputtered from separate Si and Sn targets. Si content increases from film #1 to #7.

content, for the first two cycles. First of all, all the film were produced to exhibit a similar lithiation capacity of around 0.7 mAh/cm². As shown in **Figure 19a**, the stepwise voltage plateaus, characteristic of c-Sn upon lithiation/delithiation, are clearly observed for the film with the lowest Si content. Such features appear to diminish for film #2 and #3, and almost disappear for the films with even higher Si content. The voltage profiles of films with high Si content are dominated by typical charge-discharge feature of amorphous Si when amorphous Si is the major component. Such feature evolution is even more pronounced in the corresponding
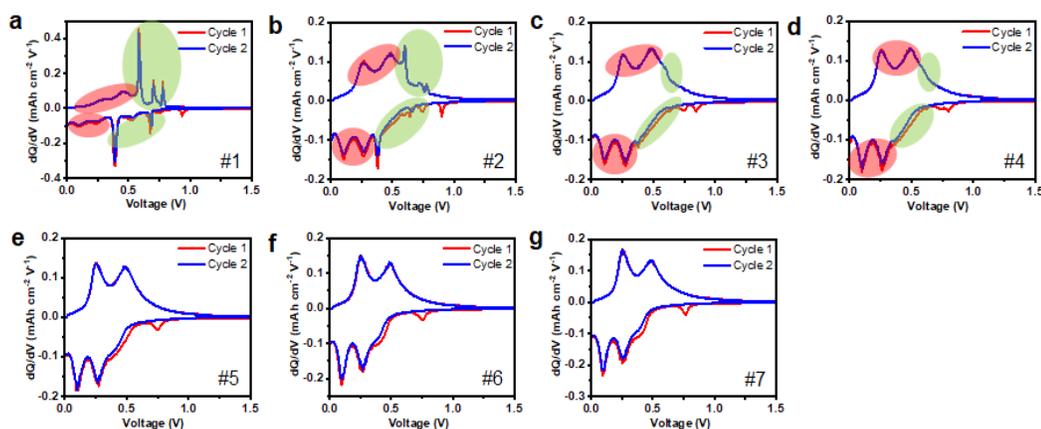

Figure 20. The dQ/dV plots of Si-Sn films co-sputtered from separate Si and Sn targets. Si content increases from film #1 to #7. Red and green highlight the amorphous and crystalline features, respectively.

dQ/dV plots of the as-produced Si-Sn thin films (**Figure 20a-g**). Correspondingly, the distinct sharp lithiation/delithiation peaks are attributed to c-Sn in film #1, which agrees well with XRD. When increasing Si content, the broad lithiation peaks below 0.3 V and delithiation peaks below 0.5 V are characteristic of amorphous Si, meanwhile, those sharp peaks relating to c-Sn is obviously present in film #2 and appears

vanishing in film #3 and #4. It can be seen that the film #5 and beyond show almost complete features of amorphous phase, confirming film #5 remains the boundary composition for amorphous film. Further studies on the cycling stability are underway to identify the optimal co-sputtering processing condition.

Conclusions

The synthesis of Si-Sn composite thin films with varied compositions on Cu foil substrates by co-sputtering two separate Si and Sn targets was pursued. The film with the highest Sn content shows XRD peaks of c-Sn, whereas the others appear X-ray amorphous. Electrochemical testing reveals the distinct features of amorphous versus crystalline as the Si/Sn ratio changes. The film morphology and composition will be studied by SEM-EDS and the electrochemical cycling performance is being evaluated to identify the optimal process condition. Such co-sputtering capability opens up the possibility to tune the film composition of varied stoichiometry and/or elements for further studies.

Improved Electrolytes for Composite Silicon Electrodes (ANL)

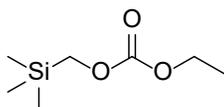M.-T.F. Rodrigues, K. Pupek, T. Dzwiniel, D.P. Abraham

Background

The energy density of lithium-ion cells can be increased by the use of silicon-containing negative electrodes. However, the long-term performance of these cells is limited by the stability of the silicon electrode-electrolyte interface, which is continually disrupted during electrochemical cycling. Hence, the development of electrolyte systems that enhance the stability of the silicon electrode-electrolyte interface is an important focus area. Electrode and cell lifetimes are strongly dependent on the electrolyte solvents, salts and additives. For example, cells with electrolytes containing $LiPF_6$ salt and conventional alkyl carbonate solvents display poor cycle life. However, the addition of fluoroethylene carbonate (FEC) and/or vinylene carbonate (VC) to these conventional systems cause remarkable improvements in cell cyclability. Specifically, these compounds facilitates formation of a robust SEI that withstands the stresses and strains induced by expansion and contraction during electrochemical cycling.
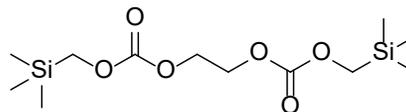
In this report, we examine electrochemical behavior of cells containing the following electrolytes:

A. 1.2 M $LiPF_6$ in TMSMEC/EMC/EC (wt. ratios 10/60/30)

B. 1.2 M $LiPF_6$ in TMSMEC/EMC/EC (wt. ratios 10/60/30) +10 wt % FEC

C. 1.2 M $LiPF_6$ in diethylene glycol bis TMSM carbonate/EMC/EC (wt. ratios 10/60/30)

D. 1.2 M $LiPF_6$ in diethylene glycol bis TMSM carbonate/EMC/EC (wt. ratios 10/60/30) +10 wt % FEC

Shown below are the structures of the TMSMEC and diethylene glycol bis TMSM carbonate compounds. These compounds were synthesized at Argonne's MERF to improve the *safety* performance of Si-containing

((trimethylsilyl)methyl) ethyl carbonate
TMSMEC

diethylene glycol bis TMSM carbonate

cells; *our objective was to examine their effect on cycling performance*. Hence, cells with 15%Si-Gr negative electrodes, and $Li_{1.03}(Ni_{0.5}Co_{0.2}Mn_{0.3})_{0.97}O_2$ positive electrodes, were assembled, tested, and compared using cycle-life aging protocols.

Results

Figure 21 shows cycle life plots for cells with the four electrolytes. The following observations are evident:

- Cells with electrolytes B and D, both containing 10 wt% FEC, have similar performance and display a capacity retention of ~54% after 100 cycles, which is similar to the capacity retention obtained with our baseline Gen 2 + 10 wt% FEC electrolyte. Hence, the safety-enhancing co-solvents do not degrade cell performance.

- Cells with electrolytes A and C have similar performance and display a capacity retention of ~10% after 100 cycles, which is similar to the capacity retention obtained with the Gen 2 electrolyte. That is, the

safety-enhancing co-solvents neither enhance nor degrade cell performance. Furthermore, it is evident that cell capacity-retention is significantly enhanced by the FEC, as noted earlier.

- The cells were also subjected to HPPC tests during cycling. The data (not shown) indicated that the impedance changes of electrolyte formulations B and D were similar, whereas those formulations A and C were similar. Furthermore, the impedance changes for the FEC containing formulations were significantly lower. These results are in accordance with the observed capacity changes.
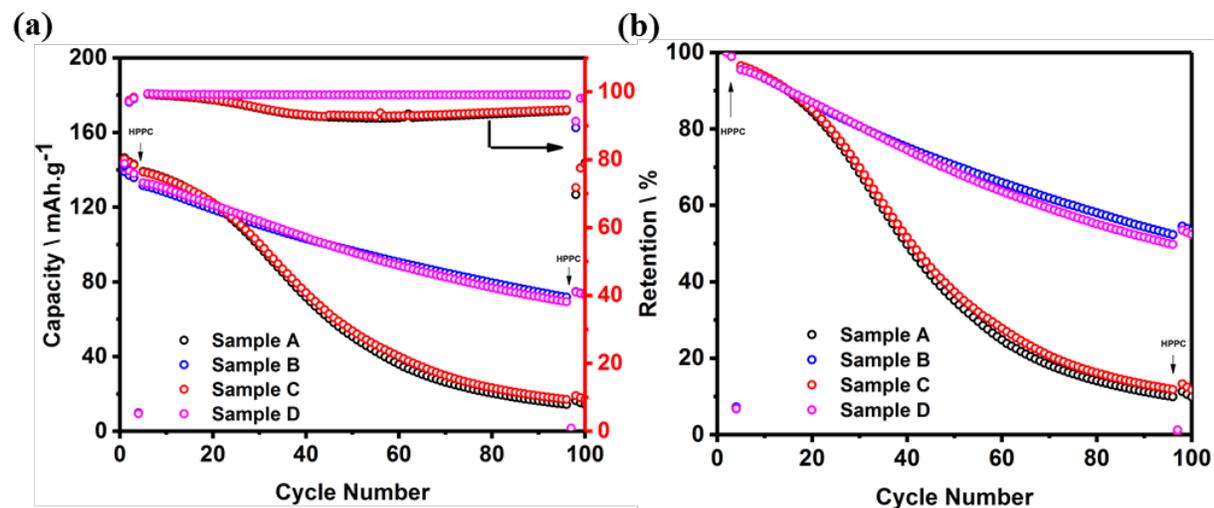

Figure 21. (a) Cycling stability and (b) capacity retention of cells with electrolytes A, B, C and D. The columbic efficiencies are shown on the right axis in (a).

Conclusions

We compared the cycle aging behavior of several cells with a NCM523-based positive electrode and a Si-containing negative electrode. The cells contained various electrolyte formulations that were developed to improve the safety performance of lithium-ion cells. Our results show that the ((trimethylsilyl)methyl) ethyl carbonate (TMSMEC) and diethylene glycol bis TMSM carbonate co-solvents neither enhance nor degrade cell cycling performance. Cells with FEC showed significantly better performance, which can be attributed to the enhanced elastomeric SEI that forms during reduction of the compound.

High Silicon Content Anodes

High Silicon Content Electrodes: CAMP Prototyping (ANL)

A.N. Jansen, S. Trask, B. Polzin, A. Dunlop, D. Kim, Joel Kirner, Wenquan Lu

Background

A small shift was made from the graphite-free efforts shown in the first quarter to developing an electrode system with more carbon-based materials to improve the electronic conductivity of the electrode matrix, while still maintaining a high-silicon content. It was reasoned that the electrode-to-electrode variations often seen are due to subtle material and processing differences that are magnified greatly by the high capacity of silicon, which is ten times the capacity of graphite. Increasing the concentration of conductive additive in these high-silicon electrodes should ensure that the silicon particles are more firmly connected to the electrode's electronic matrix during cycling. It was decided to develop electrodes with electrochemically active carbon at 23 wt.% combined with 60 wt.% Si, 2 wt.% C45 carbon additive, and 15 wt.% LiPAA binder. Two carbons were chosen for investigation: Timcal SFG-6-L flake graphite, and Kureha hard carbon. These electrodes were designed to operate with a 100 mV lithiation cutoff (vs. Li$^+$/Li) as discussed in the last quarter.

Some difficulty was encountered in coating these electrode slurries, but useful electrodes were eventually made via optimization of the coating wet gap, temperature zone profile, ventilation flow, and coating line speed. This was especially so for the SFG-6-L flakey graphite, as can be seen in **Figure** 22 for various wet gap settings. The final specifications for both of these trial electrodes are summarized in **Figure 23**.

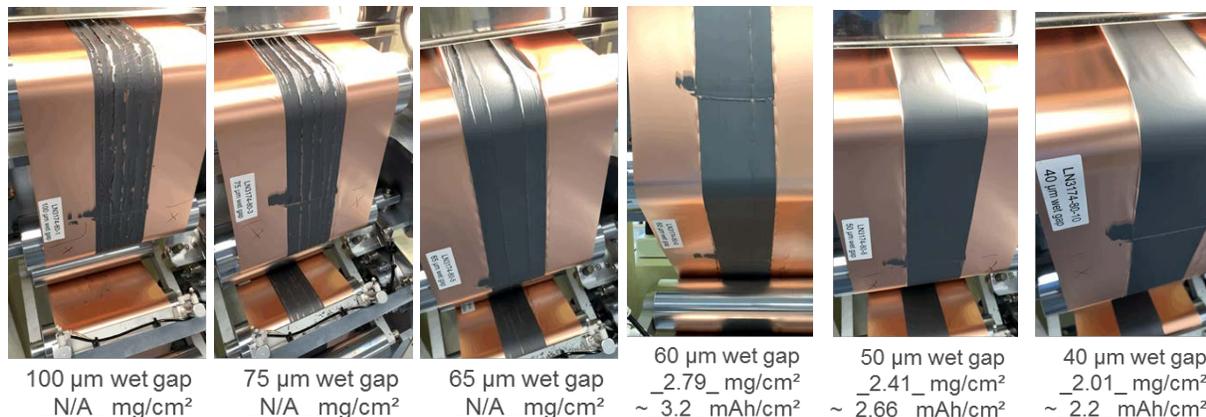| 100 μm wet gap	75 μm wet gap	65 μm wet gap	60 μm wet gap	50 μm wet gap	40 μm wet gap
_N/A_ mg/cm²	_N/A_ mg/cm²	_N/A_ mg/cm²	_2.79_ mg/cm²	_2.41_ mg/cm²	_2.01_ mg/cm²
			~_3.2_ mAh/cm²	~_2.66_ mAh/cm²	~_2.2_ mAh/cm²

Figure 22. Variations in coating quality as a function of wet gap setting for 23 wt.% SFG-6-L flakey graphite with 60 wt.% silicon.

Anode: LN3174-80-10
60 wt% Paraclete Energy nSiO "G18-031-MM"
23 wt% Timcal SFG-6-L flake graphite
2 wt% Timcal C45 carbon
15 wt% LiPAA (H2O), LiOH titrated
Paraclete nSiO [G18-031-MM], "SS" = single sided -> Calendered by hand
Cu Foil: 10 microns
Total Electrode Thickness: 28 μm (SS)
Coating Thickness: 18 μm (SS)
Porosity: 44.4 %
Total SS Coating Loading: 2.01 mg/cm²
Total SS Coating Density: 1.12 g/cm³
Made by CAMP Facility

Anode: LN3174-81-8
60 wt% Paraclete Energy nSiO "G18-031-MM"
23 wt% Kureha Hard Carbon
2 wt% Timcal C45 carbon
15 wt% LiPAA (H2O), LiOH titrated
Paraclete nSiO [G18-031-MM], Kureha Carbotron P S(F) grade hard carbon Lot#: 229601, "SS" = single sided -> Calendered by hand
Cu Foil: 10 microns
Total Electrode Thickness: 28 μm (SS)
Coating Thickness: 18 μm (SS)
Porosity: 49.0 %
Total SS Coating Loading: 1.84 mg/cm²
Total SS Coating Density: 1.02 g/cm³
Made by CAMP Facility

Figure 23. Final specification for the two trial electrodes produced in this quarter based on 23 wt.% electrochemically active carbon (SFG-6-L flakey graphite and hard carbon) with 60 wt.% silicon.

The half-cell performance of these two electrodes with 60 wt.% Si is shown in **Figure** 24 with a comparison to two recent 80 wt.% Si electrodes that are graphite-free (A-A017 "4 Kd Si" and A-A018 "Dec 2018 Si"; 10 wt.% C45 and 10 wt.% LiPAA). It is encouraging to see that the Coulombic efficiency is significantly improved for the electrode with SFG-6-L flakey graphite compared to the 80 wt.% Si electrodes. After the second cycle this Si-flakey graphite electrode has a delithiation specific capacity similar to the electrodes with 80 wt.% Si. However, the electrode with hard carbon had noticeably poor Coulombic efficiency and lower specific capacity. Future work will examine the 23 wt.% flakey graphite/hard carbon electrodes in full cells with NMC cathodes capacity matched to target ~100 mV lithiation cutoff potential for the anode. If these results continue to be promising, effort will be direct to improve the slurry mixing and coating processes for one of these electrode systems at higher capacity loadings. Additional efforts will be directed to exploring the impact of n:p ratio and cell voltage window with these electrode couples. Collaborations will continue with ORNL for their guidance on incorporating dispersants in the slurry-making process to improve electrode homogeniety based on their zeta potential studies.
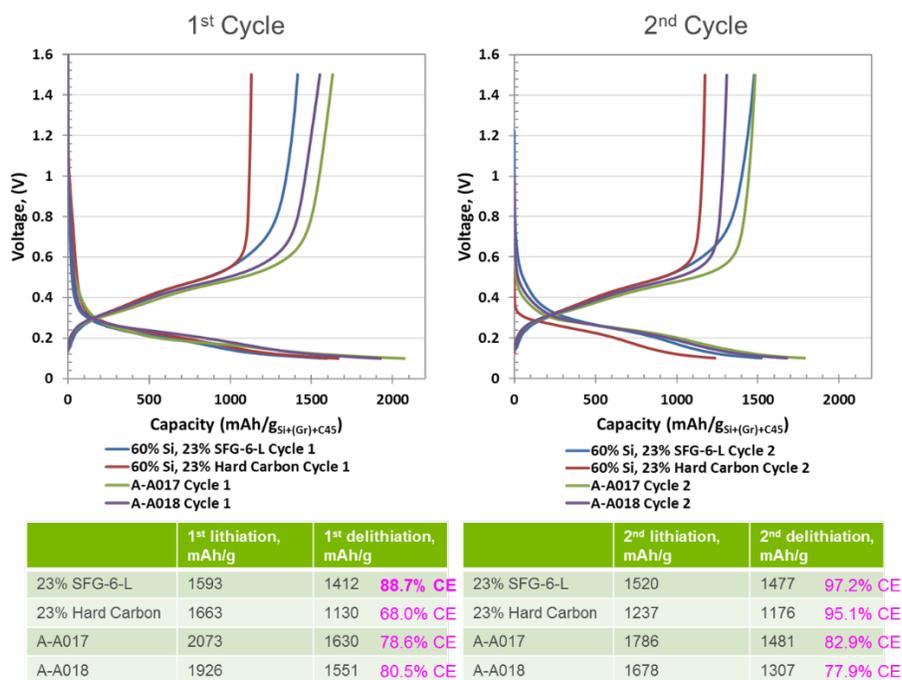

	1st lithiation, mAh/g	1st delithiation, mAh/g			2nd lithiation, mAh/g	2nd delithiation, mAh/g	
23% SFG-6-L	1593	1412	88.7% CE	23% SFG-6-L	1520	1477	97.2% CE
23% Hard Carbon	1663	1130	68.0% CE	23% Hard Carbon	1237	1176	95.1% CE
A-A017	2073	1630	78.6% CE	A-A017	1786	1481	82.9% CE
A-A018	1926	1551	80.5% CE	A-A018	1678	1307	77.9% CE

Figure 24. Lithiation & delithiation capacity versus lithium metal for 60 wt.% Si electrodes with 23 wt.% of either SFG-6-L flakey graphite or hard carbon. Comparison made to 80 wt.% graphite-free silicon electrodes (A-A017 "4 Kd Si" and A-A018 "Dec 2018 Si"; 10 wt.% C45 and 10 wt.% LiPAA), all fabricated by the CAMP Facility. These cells were cycled between 0.1 to 1.5 V vs. Li⁺/Li.

Silicon Passivation (Argonne National Laboratory)

Wenquan Lu, Joel Kirner, Linghong Zhang, Yan Qin (ANL)

Background

Batch to batch variation was observed when commercial silicon materials were electrochemically characterized at the Lab. We speculate that surface function groups on the silicon particle during the manufacturing process might be the reason for this batch to batch variation. Inspired by our previous heat treatment work on Hydro Quebec silicon particles, we conducted a series of heat treatment on these commercial available silicon particles. We found that the heat treat of the silicon particles DOES improve the electrochemical performance. The optimized heat treatment condition was also determined. This finding confirmed that surface modification of silicon material is very critical when developing silicon anode material for lithium ion batteries.

Results

The silicon particles were heat treated at various temperature from 200°C to 800°C in both air and argon gas. After the heat treatment, we first notice the color change of silicon particles, which are shown in **Figure** 25. The color of as received particle is brown. The color of the silicon powder becomes lighter and lighter with increasing the temperature for the samples heat treated in air. The color for heat treatment in argon gas is also observed. However, the color change pattern is different.

| Si as received | Air-400 | Air-600 | Ar-600 |

Figure 25   Color change of silicon powder after heat treatment

We also conducted TGA on the as received silicon particles in the air, shown in **Figure** 26. As shown in the black curve, the silicon powder was heated up to 1000°C and hold at that for 2 hours before cooling down. The blue curve is the mass change during the heat treatment. Apparently, there is a weight loss when the sample was heated to about 400oC. The weight of the sample starts to increase continuously with further increasing the temperature. The weight loss around 400°C can be attributed to the removal of the surface functional groups on the as received silicon particles, which is confirmed by FT-IR and NMR test results. The weight gain of the silicon powder above 400°C is apparently due to the oxidation reaction of silicon particle at the elevated temperature. The color of silicon particles after heat treatment shown in **Figure** 25 can be attributed to the surface change, which results from both removal of surface functional group and oxide layer formation.

All the silicon powders were made into electrode with 70% Si, 10% carbon black, and 20% LiPAA binder. The electrochemical test results are shown in **Figure** 27. The first formation voltage profiles of all the samples are shown in the **Figure** 27. It can be seen that the 1st specific capacity of silicon starts to decrease when the heat temperature is above 400°C, which could be due to the less active Si and large impedance of SiO_2 layer. However, the 3rd specific capacity of heat treated Si has a maximum around 400°C, shown in **Figure** 28 (ranging from 200°C to 500°C). The optimum heat treatment condition was determined to be 400°C in air.
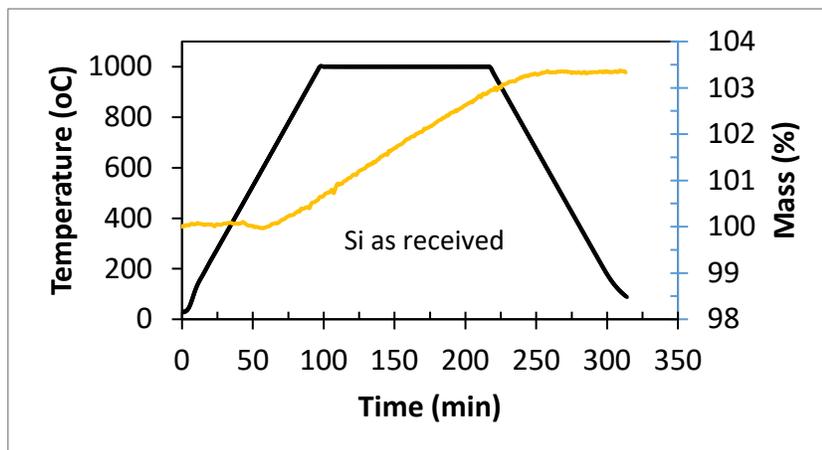
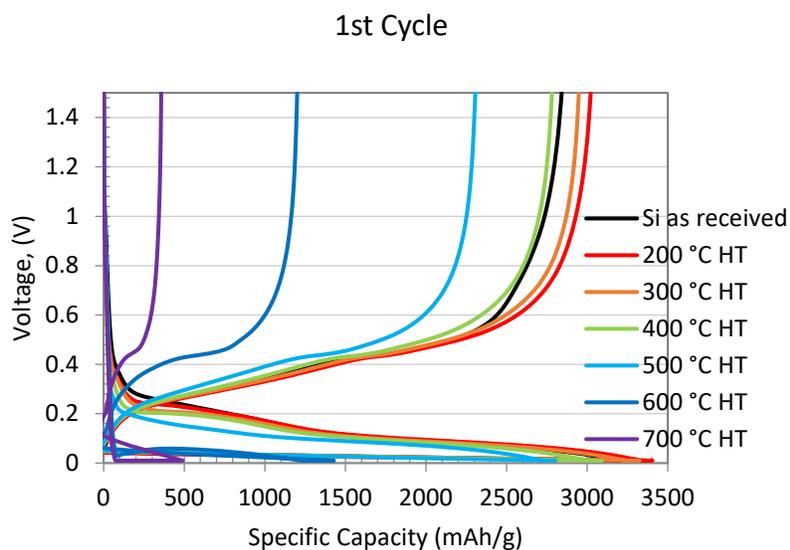**Figure** 26 Mass change of the silicon powder during heat treatment in air

Figure 27 Electrochemical performance of formation cycles for heat treated silicon powders
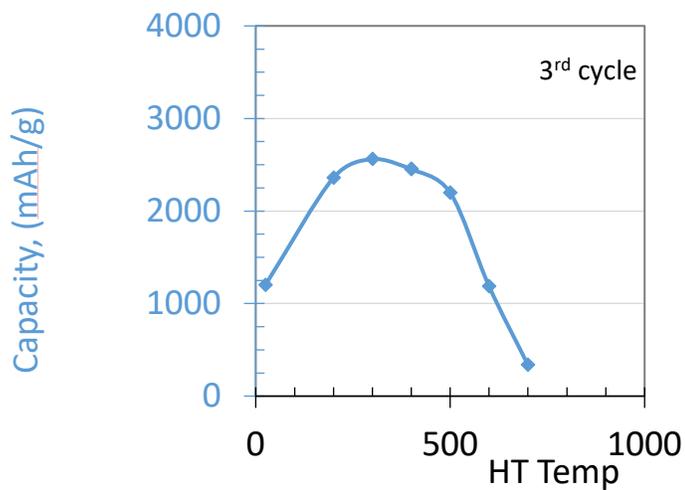
Figure 28 Electrochemical performance of formation cycles for heat treated silicon powders versus temperature

Conclusions

Batch to batch variation in terms of electrochemical performance of as received Si particles was observed. The finding of the root cause of the variation was attempted by the heat treatment the silicon particles. It is found out that the heat treatment will not only remove certain functional groups on the silicon particles, but also grow SiO_2 layer. The electrochemical performance was significantly improved by this surface modification.

High Silicon Content Electrodes Stabilized with In-situ Coatings

Binghong Han, Baris Key, Fulya Dogan, Jack Vaughey (ANL)

Background

A key attribute of a silicon electrode is the very high gravimetric capacity. This large capacity, while desirable, is associated with many other physical considerations that have hampered advancements in the field, notably high reactivity at high lithiation, volumetric growth, and uneven cation diffusion. Compared to other LIB anode systems, such as graphitic carbon, the diffusion of lithium through silicon is not very homogeneous and various studies have shown that the surface tends to be much more reduced than the bulk. Our previous studies have focused on this attribute of the electrode in that the highly reduced surface is more reactive towards the electrolyte and electrode binder than the simple state of charge would indicate. One consequence of this electronic inhomogeneity and the multitude of phases in the Li-Si phase diagram, is that the surface of the electrode is redox-active and various reactions occur that can be charge compensated by the electrode donating electrons. Our previous work with Li_7Si_3 has highlighted that the change in oxidation state can be tracked by numerous methods including X-Ray diffraction, NMR, and FTIR. Recently we noted that while the Li-Si system is redox active, similar studies using Mg-Si or the ternary system Li-Mg-Si indicate that the effect of magnesium addition appears to be to reduce significantly the available redox states of the silicon anions. **Figure** 29 shows the approximate phase diagram derived from reported structural data.
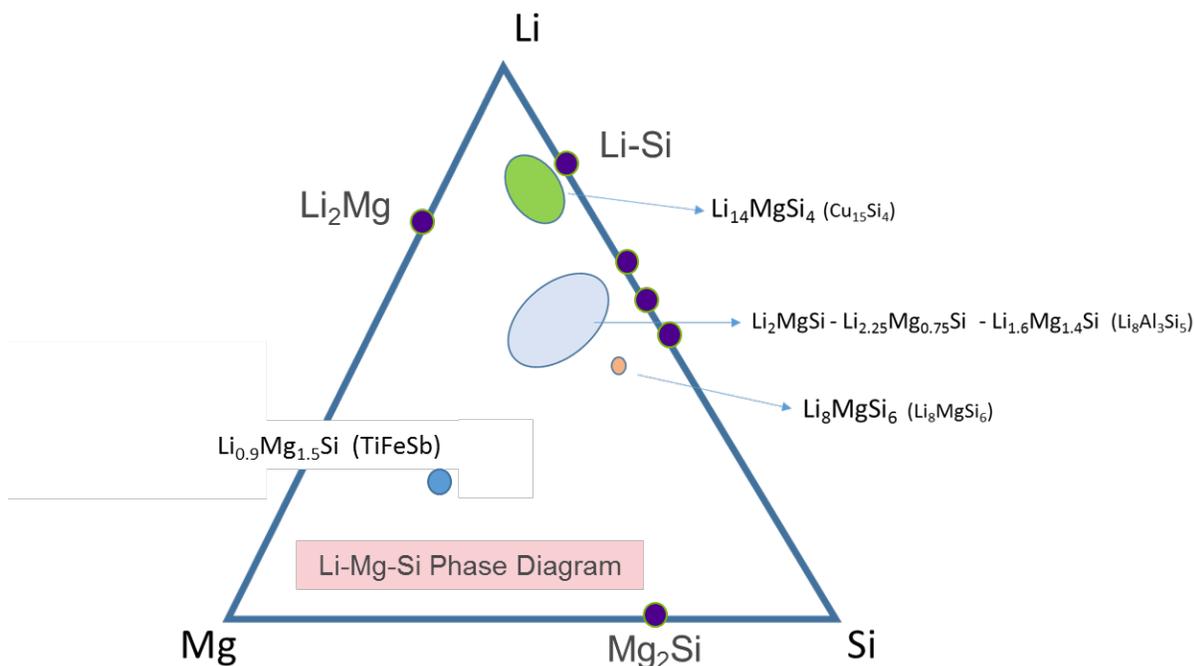

Figure 29. Approximation of the Li-Mg-Si ternary phase diagram based on reported crystallographic data

In this quarter we have synthesized model compounds in the ternary region, notably Li$_2$MgSi, and evaluated them versus common electrolytes as we had done earlier for the pure lithium silicon systems.

Results

Samples of Li$_2$MgSi were synthesized via a two-step process as recommended by Fassler et al, in his synthesis of Li$_{14}$MgSi$_4$ in 2016 (1). Initial reports by his group had noted Mg content was more homogeneous in the final products if it was first reacted with silicon to make the solid Mg$_2$Si. The Li$_2$MgSi was made from a stoichiometric mixture of lithium metal, silicon metal, and the Zintl phase Mg$_2$Si. Heating to 800 C in Ta tubes for 2h gave a black powder on cooling that was near single phase (~95%) to powder XRD.

Samples of the ternary phase were then mixed intimately with various electrolyte solvents, as had been done for the previous Li$_7$Si$_3$ studies. Samples of the solid were recovered and examined by element specific MAS-NMR studies, in this case ^{7}Li and ^{29}Si to determine phase changes (redox) from reactions with the electrolyte solvent. **Figure** 30 highlights the notable differences in the reactivity. The top two squares highlight the
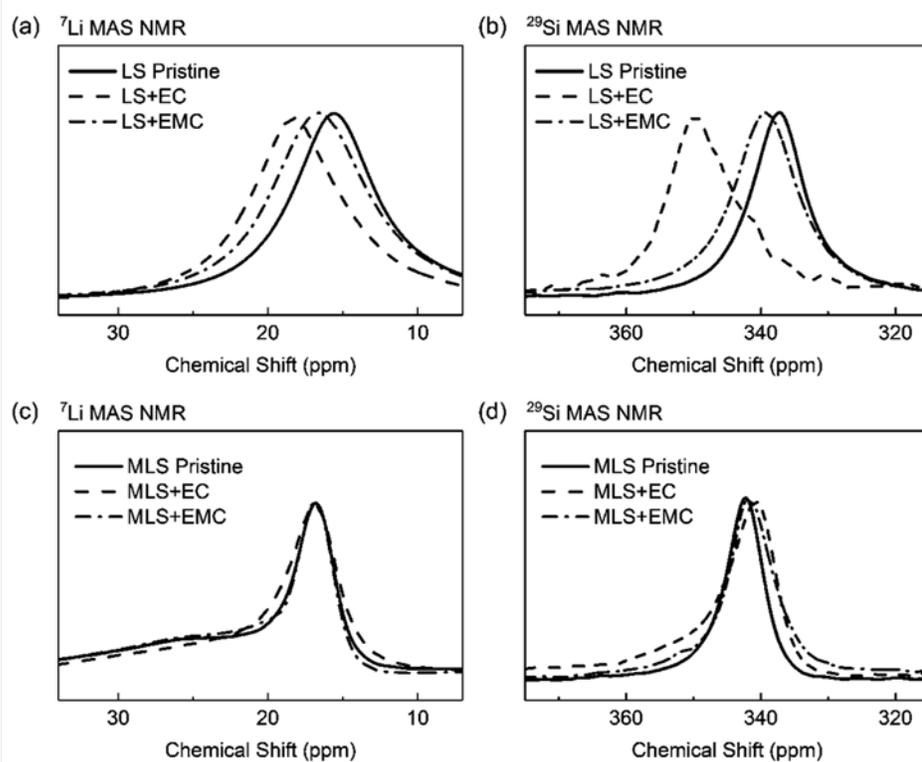

Figure 30. ^{7}Li and ^{29}Si NMR studies of the reaction products of charged anode materials with electrolyte solvents.

changes to the system with Li$_7$Si$_3$, formally a Si^{-2} compound, with changes to the silicon oxidation states noted by the peak shifts. In the case of the redox stable Li$_2$MgSi Zintl phase, under the same circumstances the more reduced Si^{-4} phase, with no changes in peak position are noted, even though the sample contains a more reactive anion.   Studies continue on alternative binder systems and the role of synthesis in controlling side reactions and the extent of reactivity.

References

1. Baran, Fassler, et al., "Substitution of Lithium for Magnesium, Zinc, and Aluminum in Li15Si4: Crystal Structures, Thermodynamic Properties, as well as 6Li and 7Li NMR Spectroscopy of Li15Si4 and Li15-xMxSi4 (M=Mg, Zn, and Al)" Chem. Eur. J. 2016, 22, 6598 – 6609

Conclusions

Based on our previous work, we have identified the surface reactivity of charged silicon electrodes as a sources of SEI formation and electrolyte instability. We have previously reported that Li_7Si_3 reacts with electrolyte to form (in part) $Li_{12}Si_7$, a slightly more oxidized lithium silicide. In this study we noted that the introduction of magnesium was found to stabilize silicon's anionic oxidation states and reduce or eliminate redox activity based on simple electrolyte reactions we had previously developed as model systems. Work continues building these phases into active electrodes.

Crack Propagation in Silicon Thin Films (NREL)

Jaclyn Coyle, Anthony Burrell, Nathan Neale (NREL)

Background

Using silicon nanomaterials is a widely accepted strategy for mitigating the extreme volume expansion associated with the lithiation of silicon and the accompanying capacity fade. However, the high surface area of silicon nanomaterials provides more opportunity for electrolyte decomposition which leads to high irreversible capacity loss and low Coulombic efficiency. Silicon microparticles are available in large scale at a low cost and offer an alternative to lower surface area and the beneficial property of a high initial Coulombic efficiency [1, 2]. However, to make silicon microparticles viable, the drastic volume change and high stress of these larger particles must be mitigated. The goal of this project is to develop a more thorough understanding of the initial lithiation mechanics of the silicon crystalline microparticles through model single crystalline electrodes. Once the fundamental fracture behavior of single crystalline silicon can be elucidated, the effect of polymer capping layers or binders in silicon composite anodes can be determined. Once the understanding of how polymer capping layers affect the lithiation depth and cracking formation of crystalline silicon, these findings may be applied to create a viable capping layer to reduce cracking in larger, more economical, silicon particles.

Results

In this quarter, we examined the morphology evolution of the Si (100) wafer electrodes during the first electrochemical cycle. For lithiation, 40 µA (100 µA cm^{-2}) of current were applied to the working electrode for 6 h using 1.2 M LiPF$_6$ in EC/EMC = 1/1 (v/v) with 10 wt% FEC electrolyte. The same current density was
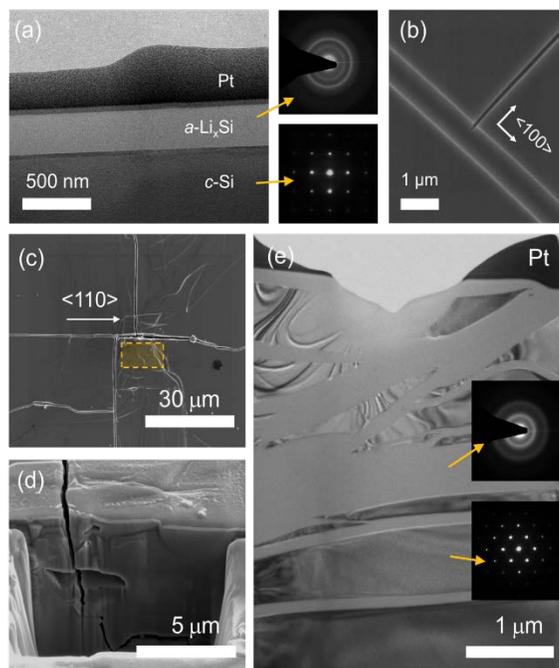

Figure 31. Morphologic study of the cracking behavior for both <110> and <100> oriented cracks (a) The cross-sectional TEM image of the flat region—where no geological deformation occurred during the previous lithiation, and the SAED patterns of the a-Li$_x$Si and c-Si layers. (b) <100>-oriented cracks observed in the flat a-Li$_x$Si layer with flat faces and sharp edges. (c) The top-view SEM image of the <110> buckled region, and (d) the cross-sectional SEM image of the <110> buckled region. (e) Cross-sectional HRTEM image and SAED patterns of the <110> buckled region.

applied for delithiation with a cutoff voltage of 1.5 V (vs. Li/Li$^+$). The TEM, SEM, SAED pattern images in **Figure 3**1 summarize the morphologic study of the crystalline silicon cracking behavior.

We found that the formation of <110>-oriented buckles—induced by the anisotropic lithiation in crystalline Si during 1st lithiation—results in cracks propagated along the <110> direction in the buckled region during 1st delithiation. Surprisingly, as the delithiation proceeds, new cracks oriented along the <100> direction appear in the intact area where no geological deformation occurred during the previous lithiation. We discovered that the <100>-oriented cracking follows the linear elastic mechanism developed for multilayer structures. By using linear elastic fracture mechanics, we have investigated the formation mechanism of <100>-oriented cracking. The results imply that the <100>-oriented cracking behavior depends on the mechanical properties of the Si substrate and the amorphous Li$_x$Si layer.

Since the end of Q2, we have continued this work on understanding the linear elastic fracture mechanics toward the Q3 progress measure "Investigate the effects of surface capping layers on mechanical stress and cracking behavior of silicon anodes." As such, we hired a new postdoctoral researcher and began a new study to modify the mechanical properties of the top surface layer of the crystalline silicon substrates by adding a polymer capping layer and observe how these polymer layers affect the electrochemically induced fractures in crystalline silicon anodes. Preliminary electrochemical data for PVDF coated and PAA coated crystalline silicon substrates is shown in **Figure 3**2. We are in the process of modifying the current densities for each polymer coating electrode to make the depth of lithiation for each electrode equivalent in order to focus solely on the effect of the mechanical properties of the surface capping layer.
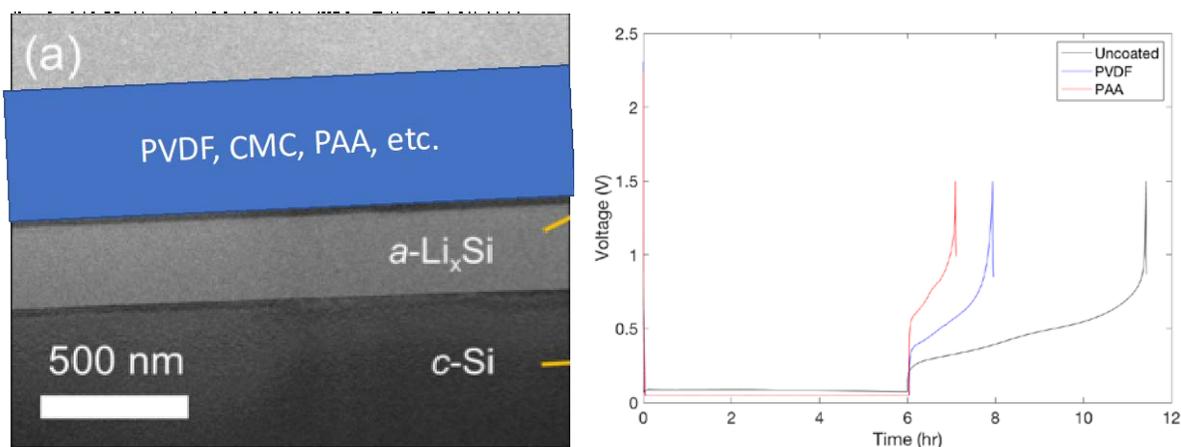

Figure 32. (a) Schematic of fracture behavior as a function of capping material. Right: First cycle lithiation and delithiation at 100 uA/cm^2 for uncoated, PVDF-coated and PAA-coated Si(100) wafer electrodes using 1.2M LiPF$_6$ in EC:EMC 3:7wt% solution with 10wt% FEC added

A notable change based on new leadership for this project is that some portion of the work being conducted via subcontract at U Kentucky has completed. We are in the process of canceling that subcontract covering work on mechanical measurements since that work has wrapped up and contributed to the aforementioned publication in preparation. These funds are being diverted to characterization necessary for Q3 & Q4 progress measures using the CU Boulder Nanomaterials Characterization Facility (http://ncf.colorado.edu), which does not require a subcontract (fee-for-use model). We will be performing focused ion beam (FIB) machining of samples enabling cross-sectional field emission scanning electron microscopy (FE-SEM) imaging in support of the Q3 and Q4 goals.

Conclusions

The findings in this work provide significant insights into the fracture behavior and formation mechanism, as well as possible strategies to inhibit crack propagations of Si electrodes at the beginning stage of cycling.

References

1.   Choi, S., et al., *Highly elastic binders integrating polyrotaxanes for silicon microparticle anodes in lithium ion batteries.* Science, 2017. **357**(6348): p. 279-283.
2.   Munaoka, T., et al., *Ionically Conductive Self-Healing Binder for Low Cost Si Microparticles Anodes in Li-Ion Batteries.* Advanced Energy Materials, 2018. **8**(14): p. 1703138.

Presentation and Publications

1.   Taeho Yoon, Chuanxiao Xiao, Jun Liu, Yikai Wang, Seoungbum Son,Yang-Tse Cheng, Chunmei Ban "Electrochemically Induced Fractures in Crystalline Silicon Anodes" *in preprartion*

Silicon Surface Functionalization (ANL)

John Zhang, Sisi Jiang, Noah Johnson (ANL)

Background

In this quarter, we continue to optimize the electrochemical performance of Si anodes using a surface ligand approach. In particular, we are developing the synthetic chemistry needed to functionalize a hydride terminated silicon surface (noted - Si-H NPs) with an epoxy-containing oligo(ethylene oxide)s of different repeating ethylene oxide unit by surface hydrosilylation. The epoxy side-group offers the chance to add a reactive group to the surface in a selective and organized way while, upon ring opening, produce a PEO-like moiety to the coating. The surface-functionalized silicon nanoparticles (noted - SF-SiNPs) demonstrate more efficient charge process and higher utilization as active materials when used as anode in lithium-ion battery probably due to the facilitated of Li$^+$ transport and better binder-particle interaction. In this quarter we report on our efforts to identify methods to scale up the Si-H precursor phase needed as an entry point to this substitution chemistry.

Results

Si Particle Surface Functionalization

SF-SiNPs featuring an ethylene oxide unit varying in chain length and epoxy group termination were synthesized as shown in **Figure** 33. When employed as active materials in silicon-graphite composite electrodes, all three SF-SiNP electrodes showed much higher initial capacities than the electrode made with non-functionalized H-SiNPs. For these materials, the Coulombic efficiency of the Si-C3-(EO)n-epoxy electrodes stabilized at 99.8% within the initial few cycles, whereas the anode with H-SiNPs never reached 99.5% prior to 80 cycles (**Figure** 34). The introduction of surface functional groups with a designed structure mitigates the surface reactivity of the Si anode and enable stable cycling performance.
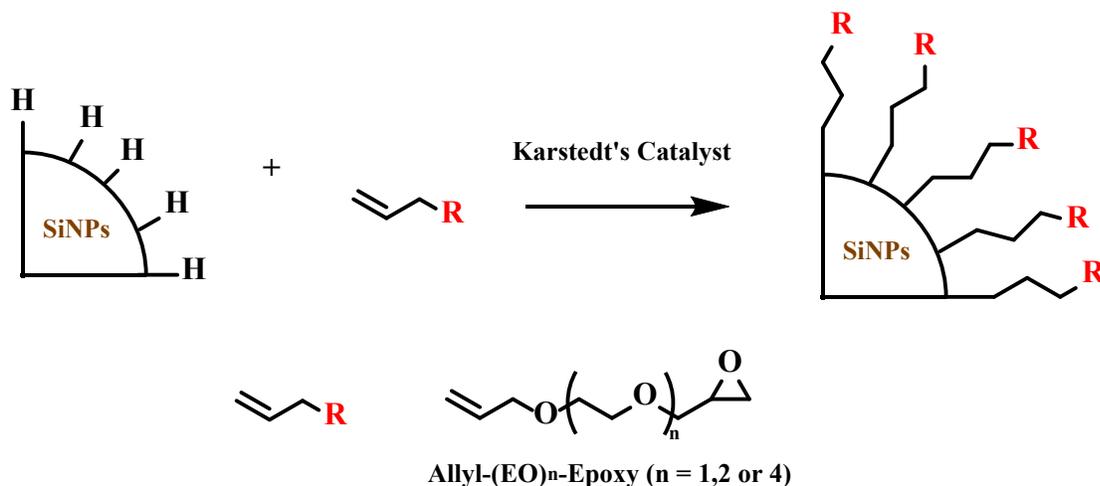

Allyl-(EO)n-Epoxy (n = 1,2 or 4)

Figure 33. Synthesis of surface-functionalized silicon nanoparticles SF-SiNPs by Pt-catalyzed hydrosilylation reaction.
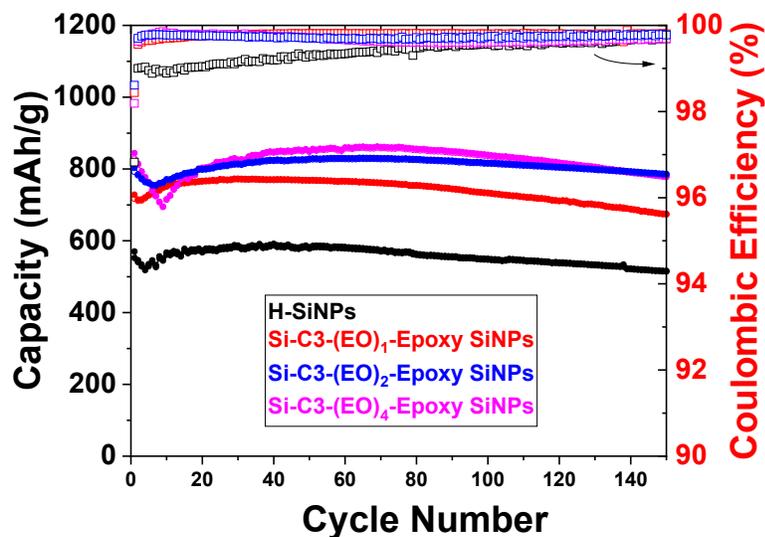
Figure 34. Capacity retention and Coulombic efficiency of Si-grahite/Li cells using H-SiNPs and SF-SiNPs as active materials, respectively. (Electrolyte: Gen 2+10 wt% FEC; C/3 for charge and discharge, cutoff voltage 0.01 – 1.5V)

Evaluation the Etching Treatment for Commercial SiNPs

Hydrofluoric acid (HF) etching treatments were conducted on four different SiNPs with varying thicknesses of silica passivation coating (Paraclete, HQ, Nano Amor and Alfa Asear). The etching condition was the same for all the samples: SiNPs were dispersed in distilled water by sonication to form a homogenous dispersion, followed by the addition of HF (50 wt % aqueous solution) in an amount in excess of the stoichiometric amount of silica reported for the sample. After etching, the particles were filtered, centrifuged and dried in vacuum oven prior to FTIR analysis. The results were shown in **Figure** 35.

The *Paraclete SiNPs* received in December 2018 are named as Paraclete_DEC18. The surface of the pristine SiNPs is covered by a native layer of SiO_2. FTIR and NMR analysis indicates Si-H and SiOH groups are also found on the particle surface together with other organic species derived from the commercial preparation process (black curve in **Figure** 35 a1). After being etched for 10 min, 20 min and 30 min, respectively, by FTIR analysis, the particles showed little difference when compared to the pristine particles. Previous FTIR analysis (red curve **Figure** 35 a2) of heated particles indicated that surface Si-H and organic species might be removed with thermal treatment (600 ºC in air by Wenquan Lu). Etching studies on these thermally treated samples indicated that the Si-H and organic ligand peaks reappeared on the FTIR spectrum of the etched particles (blue curve in 35 a2). This suggests that *Paraclete_DEC18* sample is better described as a mixture of elemental Si, SiO_2, Si-H and other organic species rather than a simple silicon particle sample with an even distribution of silica and organic surface groups.

The *Nano Amor SiNPs* with a size (vendor data) of 70-130 nm are named as *SiNA_70-130nm.* The surface of the pristine SiNPs has an inherent SiO_2 layer, Si-H, Si-OH as well as other organic groups (black curve in Figure 35b). After etching for 10 min and 20 min respectively, the FTIR peak intensity of surface Si-H, Si-OH groups increased while that of surface SiO_2 decreased, indicating the etching process did remove surface oxide. Additional analysis also indicates that the organic groups were not affected.
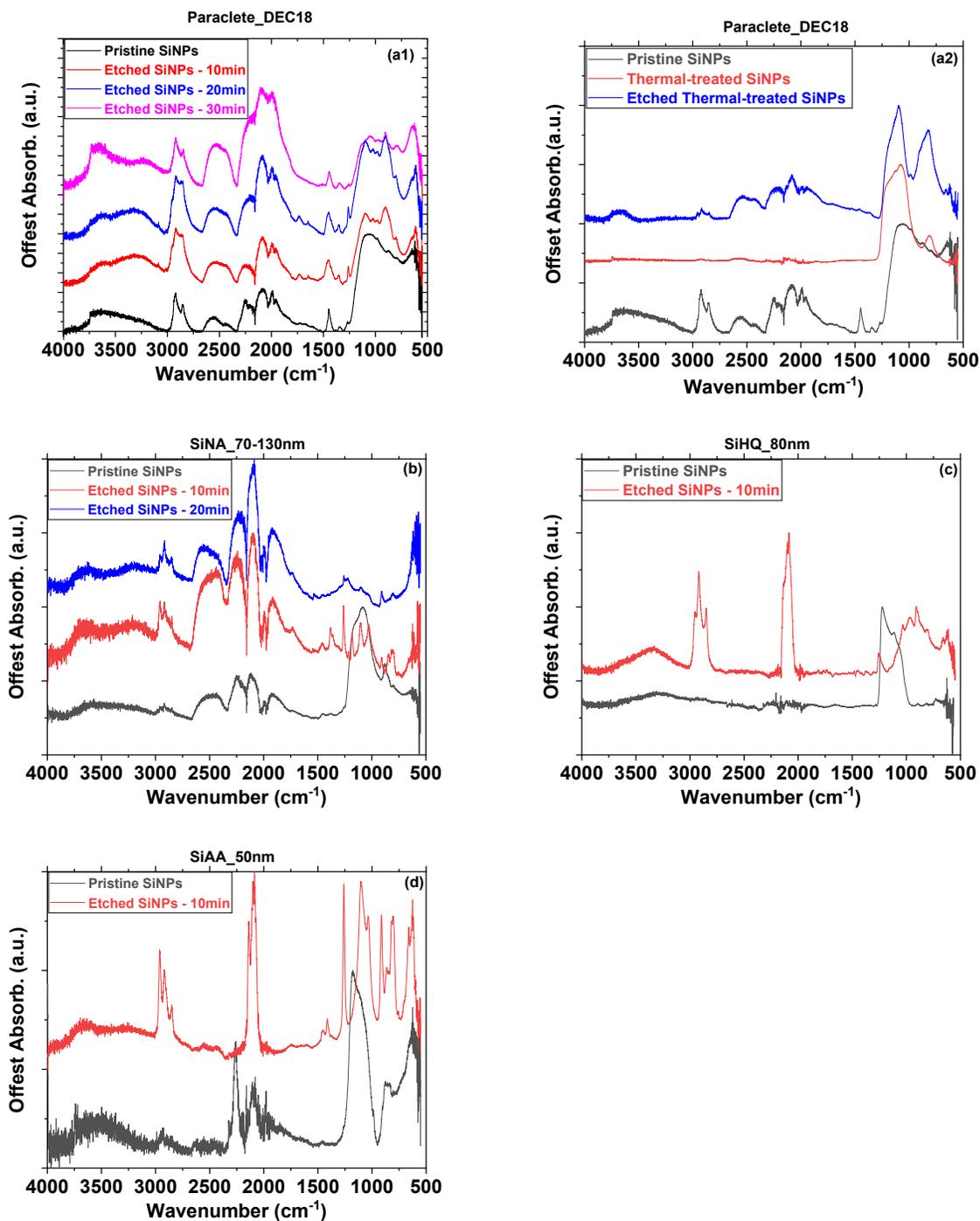
Figure 35. FTIR spectra of different commercial SiNPs before and after HF etching experiment: (a1) Paraclete, (a2) Paraclete after thermal treatment (600 ºC in air), (b) Hydroqubec (80nm), (c) Nano Amor (70-120 nm) and (d) Alfa Asear (50 nm). All the particle size provided here are vendor-claimed size.

The HQ SiNPs with a size of 80 nm (vendor data) are named as SiHQ_80nm. The surface of the pristine SiNPs was covered by a native layer of SiO2. After being etched for 10min, a Si-H peak was found in the FTIR spectrum in addition to some organic species peaks. These extra organic peaks probably correspond to

vibration bands of C-H bond of alkane groups (red curve in Figure 35c). Combined, the analysis indicates Si-H bond formation on the particle surface with the etching process exposing organic species possibly underneath the now dissolved passivation layer.

The Alfa Asear SiNPs with a size of 50 nm (vendor data) are named as *SiAA_50nm*. IR peaks of SiO_2, Si-H and Si-OH groups were found in the FTIR spectrum of the pristine SiNPs (black curve in Figure 35d). After being etched for 10min, the intensity of Si-H peak increased, the intensity of Si-OH peak decreased and new peaks corresponding to a C-H bond on an alkane group was noted.

It is worth mentioning that the peaks around 3000 cm^{-1} were observed on the FTIR spectra of all the etched particles. So far we cannot exclude the possibility that these surface organic groups comes from other sources such as reagents, containers and so on.

Conclusion

HF etching of various commercial silicon samples was attempted as a method to increase our supply of a hydride terminated silicon NP as the starting point of our surface functionalization studies. Various treatments were noted to cause differences in the recovered silicon materials, most notably the appearance of organic species and the decrease in silica content. Among the four commercial SiNPs sample, SiHQ_80nm and SiAA_50nm samples provided the most reproducible and clean H-terminated surfaces by HF etching. The surface functionalization of these two samples will be evaluated in the next quarter as our hydride silicon source.

Lithium Inventory and Diagnostics (Argonne National Laboratory)

Nasim Azimi, Zhangxing Shi, Lu Zhang, Gabriel Veith (ORNL), Christopher Johnson

Background

The lithium inventory project is morphing into an effort utilizing a rotating ring disk electrode (RRDE) design direct-drive rotating unit with bi-potentiostat is being employed. A study of the trapping of lithium in the SEI and the electron transfer and stability of the passivity of SiO_2 and Li_ySiO_x will be conducted. The following are the objectives moving forward.

(1) Determine the location of the electron transfer event during (de)lithiation: for example, at the exterior of the SEI, interior of SEI, or the interface of SEI/Si buried surface.

(2) Determine by ring voltage bias, any redox active products coming of the material as a function of voltage. The rotation speed will also allow us to probe the kinetics of the reactions.

(3) Evaluate kinetics of any 'corrosion' reactions.

(4) Measure by-products from electrochemical/chemical reactions that occur.

These four objectives are a starting point. Through these measurements, we will apply a model to describe a deeper understanding of lithium trapping and inventory loss in the SEI and near sub-surface of Si electrode.

Results

This last quarter we worked on ordering and installation of the RRDE unit and bi-potentiostat in the glovebox. (**Figure 36**). We also designed the tip-exchangeable RRDE electrodes and are currently working with Gabe Veith (ORNL) on sample preparation and characterization.

We have established collaborative efforts with (1) Gabe Veith to supply Si thin-films on Cu disk inserts for the RRDE experiments, where the ring material will be Pt; additionally, we have been working with (2) Lu Zhang (ANL), an organic chemist in the program, to supply electrolytes, electrolyte additives, and support of the project.

Figure 36. RRDE unit inside glovebox. It is capable of controlled temperature and has the capability to accept additives, redox agents via ports in the jacketed 150 mL flask for 'on the fly' electrochemical or chemical experiments.